

University of Kentucky

UKnowledge

---

Theses and Dissertations--Mining Engineering

Mining Engineering

---

2024

## AUTONOMOUS SHUTTLE CAR DOCKING TO A CONTINUOUS MINER USING RGB-DEPTH IMAGERY

Sky Rose

University of Kentucky, jboo2018@gmail.com

Author ORCID Identifier:

 <https://orcid.org/0000-0003-1974-9292>

Digital Object Identifier: <https://doi.org/10.13023/etd.2024.96>

[Right click to open a feedback form in a new tab to let us know how this document benefits you.](#)

### Recommended Citation

Rose, Sky, "AUTONOMOUS SHUTTLE CAR DOCKING TO A CONTINUOUS MINER USING RGB-DEPTH IMAGERY" (2024). *Theses and Dissertations--Mining Engineering*. 83.

[https://uknowledge.uky.edu/mng\\_etds/83](https://uknowledge.uky.edu/mng_etds/83)

This Master's Thesis is brought to you for free and open access by the Mining Engineering at UKnowledge. It has been accepted for inclusion in Theses and Dissertations--Mining Engineering by an authorized administrator of UKnowledge. For more information, please contact [UKnowledge@lsv.uky.edu](mailto:UKnowledge@lsv.uky.edu).

## **STUDENT AGREEMENT:**

I represent that my thesis or dissertation and abstract are my original work. Proper attribution has been given to all outside sources. I understand that I am solely responsible for obtaining any needed copyright permissions. I have obtained needed written permission statement(s) from the owner(s) of each third-party copyrighted matter to be included in my work, allowing electronic distribution (if such use is not permitted by the fair use doctrine) which will be submitted to UKnowledge as Additional File.

I hereby grant to The University of Kentucky and its agents the irrevocable, non-exclusive, and royalty-free license to archive and make accessible my work in whole or in part in all forms of media, now or hereafter known. I agree that the document mentioned above may be made available immediately for worldwide access unless an embargo applies.

I retain all other ownership rights to the copyright of my work. I also retain the right to use in future works (such as articles or books) all or part of my work. I understand that I am free to register the copyright to my work.

## **REVIEW, APPROVAL AND ACCEPTANCE**

The document mentioned above has been reviewed and accepted by the student's advisor, on behalf of the advisory committee, and by the Director of Graduate Studies (DGS), on behalf of the program; we verify that this is the final, approved version of the student's thesis including all changes required by the advisory committee. The undersigned agree to abide by the statements above.

Sky Rose, Student

Dr. Joseph Sottile, Major Professor

Dr. Steven Schafrik, Director of Graduate Studies

AUTONOMOUS SHUTTLE CAR DOCKING TO A CONTINUOUS MINER USING  
RGB-DEPTH IMAGERY

---

THESIS

---

A thesis submitted in partial fulfillment of the  
requirements for the degree of Master of Science in the  
College of Engineering  
at the University of Kentucky

By

Sky Rose

Lexington, Kentucky

Director: Dr. Joseph Sottile, Professor of Mining Engineering

Lexington, Kentucky

2023

Copyright © Sky Rose 2023  
<https://orcid.org/0000-0003-1974-9292>

## ABSTRACT OF THESIS

### AUTONOMOUS SHUTTLE CAR DOCKING TO A CONTINUOUS MINER USING RGB-DEPTH IMAGERY

A great deal of research is currently being conducted in automating mining equipment to improve worker health and safety and increase mine productivity. Significant progress has been made in some applications, e.g., autonomous haul trucks for surface mining. However, little progress has been made in autonomous face haulage in underground room-and pillar coal mines. Accordingly, this thesis addresses automating the operation of a shuttle car, focusing on positioning the shuttle car under the continuous miner coal-discharge conveyor during cutting and loading operations. The approach uses a stereo depth camera as the sensor, and machine-learning algorithms are used to identify various objects in the mine environment, such as the continuous miner coal-discharge conveyor, continuous miner body, roof, ribs, etc. An occupancy map is generated, a path to the continuous miner discharge conveyor is planned, and a controller is used to execute the path. The approach is developed and tested on a 1/6th-scale mock mine and in a simulated mine laboratory using full-scale equipment and manual controls.

**KEYWORDS:** Coal Mining, Autonomous Navigation, Underground Mine Face Haulage

Sky Rose

---

04/23/2024

---

Date

AUTONOMOUS SHUTTLE CAR DOCKING TO A CONTINUOUS MINER  
USING RGB-DEPTH IMAGERY

By  
Sky Rose

Dr. Joseph Sottile

---

Director of Thesis

Dr. Steven Schafrik

---

Director of Graduate Studies

04/23/2024

---

Date

## ACKNOWLEDGMENTS

I would like to acknowledge my advisor, Joseph Sottile. He was an excellent advisor and helped me figure out what to do. Without him, I would have been a disaster because being a graduate student is sometimes confusing. I would also like to thank my friends for making life just generally better.

The research reported in this thesis was supported by the National Institute for Occupational Safety and Health (NIOSH) under Contract Number 75D30120C08908. The content is solely the responsibility of the author and does not necessarily represent the official views of NIOSH.

This thesis was supported by Central Appalachian Region Education and Research Center (CARERC) through Grant 6T42OH010278. Its contents are solely the responsibility of the authors and do not necessarily represent the official views of the NIOSH/CDC.

## TABLE OF CONTENTS

ACKNOWLEDGMENTS .....	iii
LIST OF TABLES .....	vi
LIST OF FIGURES .....	vii
CHAPTER 1. INTRODUCTION .....	1
1.1 <i>Statement</i> .....	1
1.2 <i>Scope of Work</i> .....	2
CHAPTER 2. LITERATURE REVIEW .....	3
2.1 <i>Background</i> .....	3
2.1.1    Mining Background .....	3
2.1.2    Computer Science Background.....	4
2.2 <i>Current Uses</i> .....	6
CHAPTER 3. METHODOLOGY .....	9
3.1 <i>Introduction</i> .....	9
3.2 <i>Laboratory-Scale Mine and Equipment</i> .....	9
3.2.1    One-Sixth Scale Mock Mine.....	9
3.2.2    One-Sixth Scale Shuttle Car .....	10
3.2.3    One-Sixth Scale Continuous Miner .....	12
3.3 <i>Full-Scale Mine and Equipment</i> .....	14
3.4 <i>Autonomous Navigation Algorithm</i> .....	15
CHAPTER 4. DATA COLLECTION .....	17
4.1 <i>Overview</i> .....	17
4.2 <i>Cameras</i> .....	17
4.2.1    Laboratory-Scale.....	17
4.2.2    Full-Scale .....	18
4.3 <i>Image Collection</i> .....	18
4.4 <i>Annotating Images</i> .....	20
CHAPTER 5. TESTING AND ANALYSIS .....	22
5.1 <i>Introduction</i> .....	22

5.2	<i>Lab-Scale Controller</i> .....	22
5.2.1	Steering Algorithm.....	22
5.2.2	Steering Commands.....	25
5.2.3	Navigation Algorithm Performance.....	29
5.3	<i>Lab-Scale Assessment</i> .....	30
5.4	<i>Full-Scale Testing</i> .....	36
5.4.1	Full-Scale Testing.....	37
5.4.2	Full-Scale Final Assessment.....	40
CHAPTER 6. PATH PLANNING.....		43
6.1	<i>Introduction</i> .....	43
6.2	<i>Implemented Algorithm Comparison</i> .....	43
6.3	<i>A* Algorithm Development</i> .....	45
6.4	<i>A* Results</i> .....	52
CHAPTER 7. CONCLUSION.....		56
7.1	<i>Research Conclusion</i> .....	56
7.2	<i>Future Work</i> .....	57
APPENDIX.....		59
REFERENCES .....		70
VITA.....		73

## LIST OF TABLES

Table 3.1	Dimensions of Prototype Shuttle Car Compared with Joy 10SC-32B .....	12
Table 3.2	Dimensions of Full-Scale and Lab-Scale Continuous Miners.....	14
Table 5.1	Turning Radius Data.....	26
Table 5.2	Results of First Series of Tests .....	31
Table 5.3	Results of Second Series of October Tests .....	32
Table 5.4	Summary of Final Lab-Scale Tests.....	35
Table 5.5	Full-Scale Results Summary.....	41
Table 6.1	A* Evaluation Results Summary.....	53

## LIST OF FIGURES

Figure 3.1 Mock Mine with Roof Off Containing Continuous Miner.....	10
Figure 3.2 Mock Mine with Roof.....	10
Figure 3.3 One-Sixth Scale Shuttle Car Chassis.....	11
Figure 3.4 Traction Motor Mounted to Axle Gearbox .....	11
Figure 3.5 One-Sixth Scale Shuttle Car Chassis.....	12
Figure 3.6 Prototype Continuous Miner Chassis and Traction Drive.....	13
Figure 3.7 Modeled Continuous Miner.....	14
Figure 3.8 Full-Scale Environment.....	15
Figure 3.9 Block Diagram of Initial Autonomous Navigation Algorithm .....	16
Figure 4.1 Intel’s RealSense D435i Camera.....	18
Figure 4.2 ZED’s 2i Camera.....	18
Figure 4.3 Camera Tripod with Magnets.....	19
Figure 4.4 Camera Attached to Full-Scale Shuttle Car .....	19
Figure 4.5 Continuous Miner Conveyor Annotated .....	20
Figure 4.6 Continuous Miner Body Annotated .....	21
Figure 5.1 Illustration of Shuttle Car Trajectory .....	23
Figure 5.2 Plot of Measured Turning Radii for Controller Signals Ranging from 40 to 80 .....	27
Figure 5.3 Plotted Turning Radius Data at Range of 60-100cm .....	28
Figure 5.4 Plotted Turning Radius Data at Range of 100-170cm .....	28
Figure 5.5 Plotted Turning Radius Data at Range of 170-340cm .....	28
Figure 5.6 Plotted Turning Radius Data at Range of Greater than 340cm.....	29
Figure 5.7 Mirrored Trend Lines .....	29
Figure 5.8 Block Diagram of the Final Autonomous Navigation Algorithm.....	30
Figure 5.9 Start and End Positions of Shuttle Car for Test 10 of Table 5.3 .....	34
Figure 5.10 Externally Mounted Headlight to Shuttle Car Load-End.....	37
Figure 5.11 Segmented Image of Misclassified Headlight.....	38
Figure 5.12 RGB Image of Headlight.....	38
Figure 5.13 Segmented Image of Curtain .....	38
Figure 5.14 RGB Image of Curtain .....	38
Figure 5.15 Segmented Image of Person in Shuttle Car Path.....	39
Figure 5.16 RGB Image of Person in Shuttle Car Path .....	39
Figure 5.17 Incorrectly Planned Path with a Person in Shuttle Car Path .....	39
Figure 5.18 Starting Position of Representative Full-Scale Test.....	40
Figure 5.19 Ending Position of Representative Full-Scale Test.....	40
Figure 6.1 Rapidly Exploring Random Trees [12] .....	43
Figure 6.2 Representative Comparison of Path Planning Methods .....	45
Figure 6.3 RRT# Path Planning Result.....	47

Figure 6.4 A* Path Planning Result.....	47
Figure 6.5 A* Bad Path Result .....	48
Figure 6.6 A* No Path .....	49
Figure 6.7 Original Occupancy Map .....	50
Figure 6.8 Modified Greyscaled Occupancy Map.....	50
Figure 6.9 Path Avoiding Obstacle.....	51
Figure 6.10 Shuttle Car Docked Correctly Under Miner Conveyor.....	52
Figure 6.11 Shuttle Car Incorrectly Docked, Short of Conveyor .....	52
Figure 6.12 Position of CM, Obstacle, and Shuttle Car Start Position for A* Path Planner Evaluation .....	53
Figure 6.13 Start and End Positions of Shuttle Car for Test 6 of Table 6.1 .....	55
Figure 7.1 Block Diagram of Autonomous Navigation Pipeline.....	56

## CHAPTER 1. INTRODUCTION

### 1.1 Statement

Vehicle navigation and control can be, and have been, implemented using many different sensors and algorithms, e.g., radar, LiDAR, and sonar. This is especially true through global positioning system (GPS), because GPS can provide location information in real-time and be used and accessed nearly anywhere in the world. However, accurately positioning and driving vehicles becomes difficult without GPS, such as in underground mines.

In coal mining, a continuous miner cuts and gathers coal from the current working face and loads the cut coal into a shuttle car that hauls the coal to a belt feeder-breaker, which discharges the run-of-mine coal onto a conveyor belt. To be effective and efficient, the load-end of the shuttle car must be approximately centered under the continuous miner conveyor tail to prevent coal spillage. Spillage would cause delays, resulting in lost production downtime for cleanup. Therefore, accurately positioning the shuttle car is essential.

There are multiple unique challenges associated with positioning, or docking, a shuttle car with a continuous miner (CM). The vehicles are very large compared with the travel ways (entries and crosscuts) in an underground mine and the entries and crosscuts frequently run perpendicular to one another. The precise location and pose of the shuttle car in its environment with respect to its target is another major issue. Lastly how will the vehicle distinguish its target from other objects? Determining the best algorithm and sensors is important in solving these issues.

Because of the limited access to full-size mining equipment, a logical starting point is the development of a system on a small-scale mock-up of the mining environment. If successful, the approach can be scaled up to full-size equipment.

## 1.2 Scope of Work

The methodology ultimately selected for solving the autonomous navigation problem consists of using a depth camera to collect color images and depth information for object recognition and distance determination, the development of an occupancy grid of the environment, the development of a path planner to establish the path for the shuttle car to the continuous miner, and the development of a controller to execute the path. A third party was used for object classification, development of the occupancy grid, and primary path planning. Therefore, this thesis research consists of the following:

Assumption:

the continuous miner is in view of the shuttle car

Objectives:

(1) capture and annotate images of a 1/6th-scale mockup and a full-scale continuous miner in simulated mine environments,

(2) develop a controller algorithm to execute the path developed by the third-party path planner,

(3) test and evaluate the autonomous navigation pipeline, and

(4) develop and test an alternative path planner.

## CHAPTER 2. LITERATURE REVIEW

### 2.1 Background

#### 2.1.1 Mining Background

The use of autonomous vehicles in industrial and consumer applications has been in development for several decades. Examples include transportation and logistics, agriculture, construction, and mining. The health and safety of workers are the primary motivators for automation in mining.

In most industrial applications, automation is implemented to remove people from repetitive and/or dangerous tasks. Repetitive tasks can cause worker fatigue, which can reduce attention, impair judgement, and slow reaction times, resulting in severe injury or death. Automation can be applied to execute tasks for long periods precisely and without fatigue. By employing automation in the mining industry, operators can become supervisors of the machines, removing themselves from hazardous environments or repetitive tasks.

In mining, the biggest motivator in introducing/using automation is to improve miner health and safety. Considerable effort has been made to increase miners' health and safety throughout history; however, working in underground environments still includes many hazards. In coal mining, current working sections are particularly hazardous because of large mobile equipment operating in confined, low-lighting spaces near workers. This has unfortunately caused many miners to suffer serious injury or death. From 2018 to 2022, there were 49 fatalities in US coal mines. The Mine Safety and Health Administration (MSHA) reported that 33 of those fatalities occurred underground, with 18 being classified as Machinery and Powered Haulage incidents [1]. An example of a recent fatality occurred

on June 3rd, 2021, when a West Virginia mine foreman was struck and killed by a shuttle car while he was walking through an intersection. An evaluation showed that “the load of coal on the shuttle car obstructed the shuttle car operator’s view of the offside of the machine at the time of the accident” [2].

Burgess-Limerick and Steiner [3] conducted a study that analyzed the injuries surrounding mobile equipment in underground coal mines in New South Wales from 2002 through 2005. In that period, 959 injuries occurred from continuous miners, shuttle cars, load-haul-dump (LHDs), and personal transport vehicles. Although there were occasions where miners were struck by, or caught in between the machinery, most of the incidents were strains or incidents getting in/out of the equipment. For shuttle cars, the majority of incidents were from strains or operating on rough mine floors [3]. Many of these incidents could have been caused by fatigue from working long hours at labor-intensive, repetitive tasks. Repetitive tasks cause muscles to become tired, resulting in decreased performance. Repetitive tasks can cause mental fatigue as well. Lack of sleep is another source of fatigue. Some miners work 12-hour shifts and may also have long commute times. It was reported that miners with sleep problems have an average of almost twice a higher risk of being injured compared with miners without sleep problems. Fatigued and tired miners can lose their situational awareness and make poor decisions [5].

Thus, relieving miners of repetitive tasks, to enable them to supervise autonomous equipment would be favorable for the betterment of their health and safety.

### 2.1.2 Computer Science Background

Autonomously navigating a vehicle requires a path planning algorithm that will correctly take the vehicle to a specified waypoint in the shortest practical path. There have been numerous base and variant algorithms created in the past several decades that can

achieve this goal. A few examples are rapidly exploring random trees sharp (RRT#), transition-based rapidly exploring random trees (TRRT), and A\* (pronounced A star). RRT# and TRRT are variants of the base algorithm, rapidly exploring random trees (RRT); therefore, RRT will also be discussed.

RRT is a concept initially theorized and developed by LaValle in 1998, designed to specifically address situations where an agent or vehicle has constraints in its position and movement [6]. RRT will first pick a random node between the starting node and a node up to a user-defined maximum distance. It will check the location of the random node and compare if the node is within the bounds of an obstacle. It will connect the node with its nearest neighboring node, but if the node is in the bounds of an obstacle, then the node will be ignored. To confirm completion, RRT will check if the current node is within the bounds of the target.

RRT# is an improvement of RRT, created by Arslan and Tsiotras in 2012, with a focus on a consistent spanning tree. RRT# behaves the same as RRT; however, with one exception: information about the lowest cost path (the shortest distance between nodes) is stored in the abovementioned consistent spanning tree. This produces better efficiency as the range of nodes to search is narrower compared with RRT [7].

TRRT is another variant and improvement of RRT, created by Jaillet, et al in 2008, with the focus of integrating stochastic optimization methods. Based on the stochastic optimization methods, TRRT assigns states to nodes and accepts them, or ignores them, based on the ease of navigation from their nearest neighbors. This approach does not create an optimal path to the goal; however, it creates a path more quickly than RRT [8].

A\* is a pathfinding algorithm theorized and created by Hart, et al. in 1968. It was created as part of a project to build a robot that could plan its own path/actions [9]. A\* is a popular path-searching algorithm because of its ability to find the shortest paths efficiently. Due to its simplicity, the coordinates of the starting point and the target are given to A\* at the start. Beginning at the start node, A\* finds a neighboring node with the smallest cost (estimated shortest distance or time from a heuristic function) and connects them. A\* can connect to neighboring nodes in four directions (0°, 90°, 180°, 270°) or eight directions (0°, 45°...), the mode of movement depends on the choice of the user. It iterates this process and connects the neighboring nodes until the current node is the target [10].

## 2.2 Current Uses

An early example of autonomous navigation in underground mines was an experiment done by Scheduling, et al. in 1999 [11]. The experiment focused on sensor testing and navigation vehicle models on LHDs. They mainly focused on two navigation models, one with wheel slip during motion and one without wheel slip. It was found that the model with wheel slip incorporated, due to heavy machinery and harsh uneven terrain, was the better model with an inertial navigation system and a time-of-flight laser scanner as a redundancy check.

Another early example of autonomous navigation in underground mines was an experiment done by Dragt, et al. in 2003 [12]. This experiment also focused on navigation methods for LHDs. The navigation methods included the following: absolute navigation and reactive navigation. It was found that the better method for absolute navigation was simultaneous localization and mapping (SLAM) logic [12]. This result was important because it requires no extra infrastructure in the mine, new routes are simple and take little

time to generate, remote control operation was integrated seamlessly into the algorithm, and the LHD could drive at full speed without needing to reduce speed to update data. The best reactive navigation method was found to be a wall following approach. Unlike the absolute navigation method, the reactive navigation method does not need to keep a frame of reference and only needs to react to objects in the immediate vicinity. However, there are issues with both absolute navigation and reactive navigation. Absolute navigation requires a high computing cost and localization errors accumulate, causing the algorithm to easily lose its frame of reference. Reactive navigation cannot look ahead of its current position, making it difficult to position the vehicle correctly for making turns. They concluded that an algorithm combining absolute navigation and reactive navigation would be best for the dynamic environments in mining.

Many current forms of automation involve the use of GPS; however, due to being underground, GPS cannot be used. To deal with this, Losch, et al. designed and created a robot that can autonomously navigate through underground mines via attached sensors [13]. The robot was equipped with an XSens MTi-30-AHRS-2A5G4 inertia system, a Microsoft Kinect camera for localization, and other sensors. Given known terrain, the robot was able to traverse autonomously through rough, non-straight, and dark environments. However, the work was never applied to mining equipment.

There have been instances where autonomy has been applied to shuttle cars. Francis Enterprises, Inc. developed a prototype that allows for remote control of a full-scale shuttle car [14]. The prototype provides real-time imagery from cameras attached to the shuttle car, while controller inputs and responses are sent through the shuttle car's trailing cable. Using the remote-control prototype, Francis Enterprises, Inc. also developed

a shuttle car prototype that is fully autonomous [15]. An 800-foot path was able to be mapped and navigated using their prototype.

Lastly, Agioutantis, et al. developed a framework to autonomously control a shuttle car using four LiDAR sensors [16]. Their framework was applied to a shuttle car in both lab-scale and full-scale simulated mine environments and was demonstrated to successfully develop and map and autonomously navigate a shuttle car in the environments.

## CHAPTER 3. METHODOLOGY

### 3.1 Introduction

This chapter will describe the laboratory-scale and full-scale mine equipment and environments used in this research. A brief overview of autonomous navigation pipeline will also be provided.

### 3.2 Laboratory-Scale Mine and Equipment

The laboratory environment used for the development and preliminary testing of the autonomous navigation system consisted of a 1/6th-scale mock model of a coal mine including an intersection, a 1/6th-scale shuttle car capable of being remotely and autonomously controlled, and a 1/6th-scale model of a remotely controlled continuous miner. Because the mock mine and equipment were previously built and available for this research [17], only an overview of the relevant specifications will be given.

#### 3.2.1 One-Sixth Scale Mock Mine

The mock mine consisted of a floor, ribs, and roof assembled from sheets of plywood painted flat black to simulate the mine environment. The ribs were cut to a height of 16 inches, which equates to an eight-foot coal seam. Crosscuts and entries were 40 inches wide, corresponding to a 20-ft width. The mock mine included a crosscut to allow for testing with the continuous miner in the straight, turning left, and turning right. A photo of the mock mine with the CM (described later) is shown in Figure 3.1. Figure 3.2 shows the mine with the roof placed on top of the ribs to darken the environment.



Figure 3.1 Mock Mine with Roof Off  
Containing Continuous Miner



Figure 3.2 Mock Mine with Roof

### 3.2.2 One-Sixth Scale Shuttle Car

The shuttle car chassis was constructed with parts from a remote-controlled (RC) car. Two identical axles from the RC car are connected by two pieces of angle aluminum, forming the chassis, shown in Figure 3.3. An enclosure between the aluminum pieces houses electronic components, also shown in Figure 3.3.

Tramming of the shuttle car is accomplished by two 24 V brushless dc (BLDC) planetary gear motors (LRPX32-090V24-000-X003 manufactured by ElectroCraft) mounted to the gearbox of each axle, shown in Figure 3.4. The traction motors are controlled by a Roboteq SBL2360, 60-V 2x20, a dual BLDC Motor Controller. The motor's continuous running speed is 8,000 rpm. The planetary gear provides an additional speed reduction of 3.21, making the continuous running speed of the motor shaft 2,489 rpm. With the 63.75 speed reduction from the gearbox and axle, the wheel speed at continuous running rating is 39 rpm. This provides a linear speed of 41.5 cm/s, or a relative speed of 3.4 seconds to travel the length of the shuttle car. Considering the length of 9.08 m for a full-scale shuttle car and the statutory speed limit of 6.0 mph (9.66 kmph), the maximum relative speed of a full-scale shuttle car is 3.3 seconds to travel its length. Therefore, the tramming capabilities of the scale model match well with the full-scale shuttle car.



Figure 3.3 One-Sixth Scale Shuttle Car Chassis



Figure 3.4 Traction Motor Mounted to Axle Gearbox

Steering is four-wheel, opposite-direction steering, which matches the type of steering used in full-scale shuttle cars. Steering is accomplished through four servomotors, two mounted above each axle and connected to tie-rods. The servomotors are controlled by standard RC pulse-width modulation (PWM) signals generated by an Arduino Uno. A python script is used to produce pulses to produce the desired turn radius.

The body was 3D printed based on a Joy 10SC-32B shuttle car from Komatsu. An Intel RealSense D435i camera was attached to the shuttle car. No decision was made in the selection of this camera because it was determined in a previous project [17]. An additional light was used and placed on top of the shuttle car near the camera because the shuttle car headlights would be under the conveyor when the shuttle car was near the continuous miner, preventing illumination of the conveyor tail.

The constructed shuttle car is presented in Figure 3.5, and Table 3.1 provides a comparison of dimensions of the 1/6th scale model with the Joy 10SC-32B shuttle car. The comparison shows that all dimensions, except for the tires, are very close to the target of 1/6th scale.



Figure 3.5 One-Sixth Scale Shuttle Car Chassis

Table 3.1 Dimensions of Prototype Shuttle Car Compared with Joy 10SC-32B

Parameter	Joy 10SC-32B, cm	Prototype, cm	Scale Factor
Length	908	144.8	0.16
Width	340.4	50	0.15
Wheelbase	290	48	0.17
Tire Diameter	74	20	0.27

### 3.2.3 One-Sixth Scale Continuous Miner

Having to be able to reproduce the movements of a full-scale continuous miner, the model continuous miner chassis, crawler frame, and crawlers were assembled from an RC excavator and aluminum bars, shown in Figure 3.6. The RC parts allow for independent speed and direction control of each crawler on the 1/6th scale continuous miner.

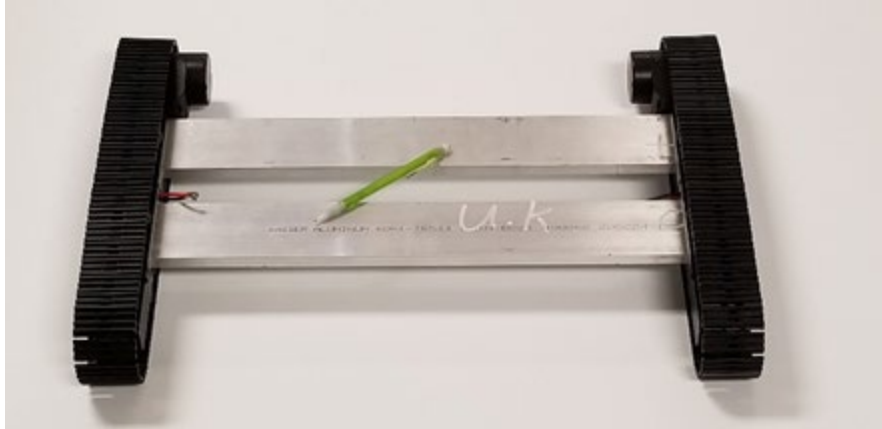


Figure 3.6 Prototype Continuous Miner Chassis and Traction Drive

The continuous miner is composed of four major parts: the body, coal conveyor assembly, gathering head, and ranging arm/cutting drum. These parts were 3D printed from drawings made in Autodesk Fusion 360. No mechanical drawings of a continuous miner were available, so a representative model was developed from specifications and drawings based on Caterpillar's CM445 and Joy Global's 12CM12, found on their websites. Because a 1/6th scale continuous miner is quite large (close to two meters long), requiring a large amount of filament to print, each major part was split into several component parts and printed separately to minimize the amount of support fill required during the printing process. The body included an enclosure for the battery and electronics and an enclosure for the hydraulic pump and reservoir to raise and lower the conveyor.

The constructed continuous miner is shown in Figure 3.7, Table 3.2 shows a comparison of the dimensions of the lab-scale continuous miner with the dimensions of a representative continuous miner.

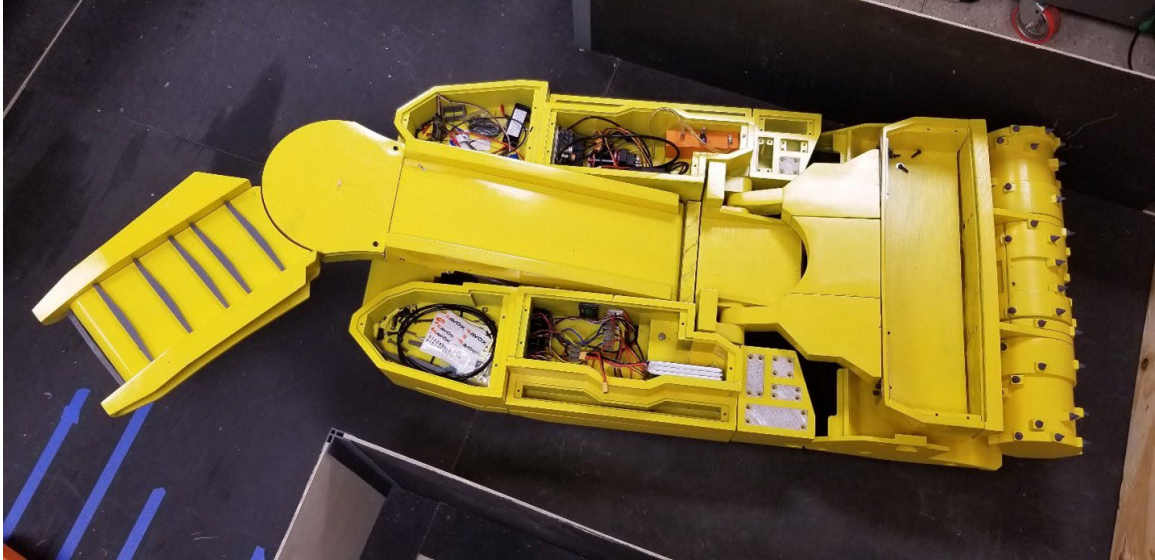


Figure 3.7 Modeled Continuous Miner

Table 3.2 Dimensions of Full-Scale and Lab-Scale Continuous Miners

Parameter	Full Scale, m	Prototype, m	Scale Factor, avg
Length	10.50 – 11.0	1.81	0.165
Width	3.20 – 3.50	0.64	0.19
Height	1.30 – 1.50	0.22	0.16

### 3.3 Full-Scale Mine and Equipment

A full-scale environment was used for final testing of the autonomous navigation algorithm. West Virginia Training and Conference Center, in their simulated mine lab, was the location for full-scale testing. This location was chosen because it is the only facility available with access to full-scale operational equipment.

The simulated mine lab is a room and pillar mine layout consisting of 20x20-foot pillars and 20-foot-wide entries and crosscuts, forming eight entries and seven crosscuts. In addition, the simulated mine lab also contains mining equipment including a shuttle car, a continuous miner, cables, ventilation curtains, and roof bolter. An image showing the full-scale environment is shown in Figure 3.8.



Figure 3.8 Full-Scale Environment

### 3.4 Autonomous Navigation Algorithm

Autonomous navigation enables a vehicle to determine its location and plan and follow a path automatically, i.e., without human intervention, to a given target. The vehicle must navigate the planned path while continuously avoiding obstacles.

A SLAM-based navigation algorithm was created by SRI International to implement autonomous navigation in lab-scale and full-scale settings [19]. It included an initial step that uses RGB and depth information taken by a stereo camera mounted on the shuttle car as a known location. The image is then segmented into different objects, based on the pixels they contain, and automatically labeled via a custom segmentation neural network. From this, and depth information, the locations of various objects in the environment and the continuous miner conveyor tail are estimated. An occupancy map is then created by flattening the 3D depth information onto a 2D plane. Using the occupancy map and the CM location, a path is determined, and trajectory vectors (distance and angle)

are exported. This research involved testing and evaluating this pipeline, developing the external program/interface to control the shuttle car to the waypoints given by the algorithm, and the development of an alternative path planner. Note that this pipeline runs continuously. A visual representation of the pipeline is displayed in Figure 3.9.

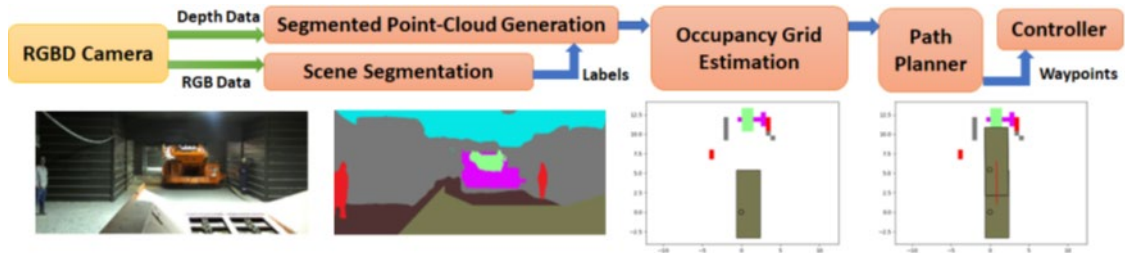


Figure 3.9 Block Diagram of Initial Autonomous Navigation Algorithm

## CHAPTER 4. DATA COLLECTION

### 4.1 Overview

In the navigation algorithm, a neural network is used to determine the location of the continuous miner conveyor tail and plan a path to it (as discussed in Chapter 3). The neural network was initially trained with RGB-Depth images that were taken using the mock mine. However, the mock mine was built at a 1/6th scale and only contained minimal objects and equipment: the continuous miner, the shuttle car, a 12-inch figure of a person, roof, and ribs.

Following this, full-scale images were taken to enhance the robustness of the navigation algorithm. Additional items, e.g., power cables and ventilation curtains that were not in lab-scale are included in the full-scale images.

### 4.2 Cameras

#### 4.2.1 Laboratory-Scale

Intel's RealSense D435i depth camera, Figure 4.1, was used in lab-scale development and testing. Specifications of the camera include a range of up to ten meters, with an ideal range of 0.3-3.0 m, a frame rate of up to 90 frames per second, and image resolution of up to 1280 pixels wide by 720 pixels high. The camera also includes an inertial measurement unit (IMU) for reporting orientation and acceleration.



Figure 4.1 Intel's RealSense D435i Camera

#### 4.2.2 Full-Scale

ZED's 2i stereo camera, shown in Figure 4.2, with a four-millimeter lens, was used for full-scale testing. Specifications of the camera include a range of up to 35 m, a frame rate of up to 100 frames per second, and image resolution of up to 2048 pixels wide by 1080 pixels high. The ZED 2i camera also includes an IMU.



Figure 4.2 ZED's 2i Camera

#### 4.3 Image Collection

The placement of the camera on the lab-scale shuttle car was in front of the operator's platform. This was done because it corresponds to the canopy location of a center-drive shuttle car, providing the best protection and point of view for center-drive shuttle cars [17].

The full-scale shuttle car is an end-drive shuttle with the operator's canopy on the standard side; however, the camera was positioned near the middle of the shuttle car on the offside, the same location as lab-scale. This position was chosen to prevent additional work and time on training the neural network from a new point of view.

The camera was mounted on the shuttle car using a tripod. However, the potential problem of using a tripod on the shuttle car was stabilization during tramping. The solution was to use switchable magnets to firmly attach the tripod to the shuttle car body, shown in Figure 4.3. This allowed the shuttle car to be trammed without worrying about camera stabilization, shown in Figure 4.4.



Figure 4.3 Camera Tripod with Magnets



Figure 4.4 Camera Attached to Full-Scale Shuttle Car

During image collection, over 400 images were gathered at various distances and angles between the shuttle car and the continuous miner. Many images were also gathered having the continuous miner turning a crosscut both to the left and the right. These images included the mine roof, cables, and ventilation curtains.

#### 4.4 Annotating Images

Image annotation is important and required for vision-based algorithms to identify the objects correctly. If the algorithm is not trained with annotated images, there is a chance that it could identify, for example, an image of a person as a section of a ventilation curtain. This problem is extremely dangerous for autonomous vehicles because it could lead to miner fatalities.

Classifying objects correctly during the annotation process is also important. Just labeling the entire image as one object would not be adequate in this application because the algorithm needs to identify the exact location of the continuous miner conveyor tail to calculate an accurate path. Therefore, images were annotated via bounding boxes and/or polygons with their respective labels for each object. An example of an annotated image with bounding polygons is shown in Figure 4.5 and Figure 4.6.

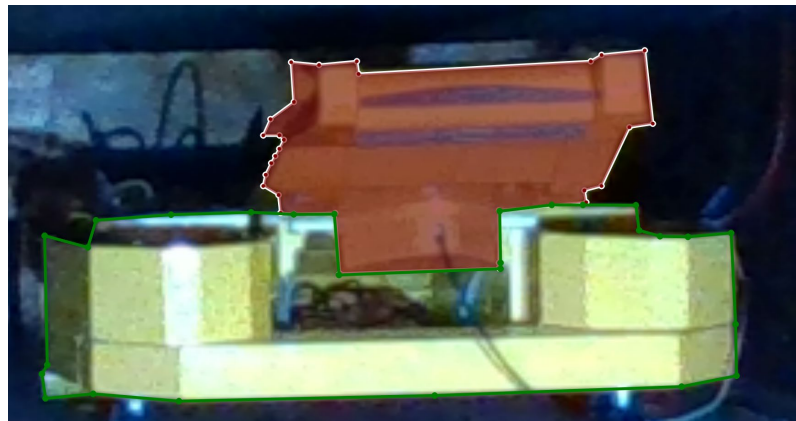


Figure 4.5 Continuous Miner Conveyor Annotated

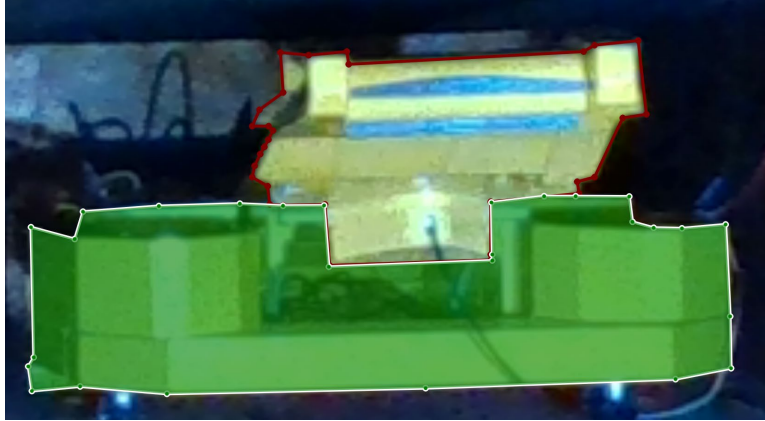


Figure 4.6 Continuous Miner Body Annotated

All images were annotated using the program Labelme, an open-source image annotation tool developed by the Massachusetts Institute of Technology's Computer Science and Artificial Intelligence Laboratory [20]. Using Labelme, polygons are layered on top of an image and assigned labels. In Figure 4.5, the conveyor tail of the continuous miner has been surrounded by the red polygon, labeled as tail, and the body of the continuous miner has been assigned the green polygon, labeled as body, in Figure 4.6. SRI International used these labeled images to train the object recognition algorithm and develop the navigation pipeline for testing and evaluation.

## CHAPTER 5. TESTING AND ANALYSIS

### 5.1 Introduction

As previously mentioned, development and testing were conducted at both lab scale and full scale. This chapter provides an overview of the development of the lab-scale controller, the results of lab-scale testing, and the results of full-scale testing.

### 5.2 Lab-Scale Controller

The lab-scale controller was designed and developed to convert the trajectory vectors (distance and angle) to waypoint coordinates and generate control signals to tram the shuttle car to each waypoint.

#### 5.2.1 Steering Algorithm

It was impractical to attempt following the straight-line trajectory provided by the path planner (unless the shuttle car body were aligned with the trajectory). Instead, it was determined that the most effective approach would be to use the trajectory vector to define the coordinates of the waypoint and tram the shuttle car to those coordinates along a smooth arc, defined by the radius of a circle.

Figure 5.1 illustrates the approach. The two dashed rectangles represent the shuttle car start and end positions for each waypoint. The frame of reference uses the centroid of the shuttle car as the origin with the x and y axes aligned with the shuttle car as shown in the figure. The approach uses the equation of a circle from three known points on it. From this equation, the radius is used to establish the angle that the shuttle car wheels should be turned to tram to the next waypoint.

Note that Figure 5.1 shows two circles. It was necessary to define both because the steering control is based on the vehicle centroid; however, the algorithm must be designed to control the position of the center of the load end of the shuttle car, which is along a different arc than the shuttle car centroid. The process is illustrated with an example.

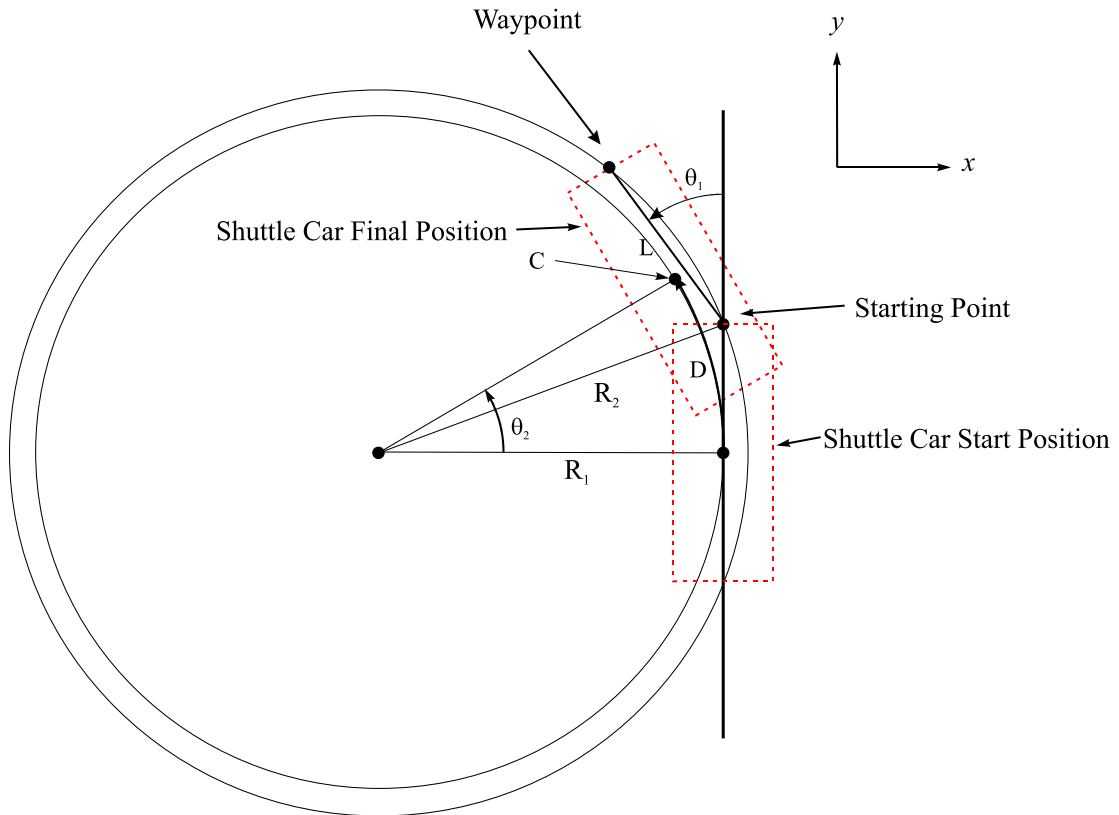


Figure 5.1 Illustration of Shuttle Car Trajectory

Consider that the shuttle car is at the start position (as shown in Figure 5.1) and it is to follow a trajectory of  $L = 55$  cm at  $\theta_1 = -12.0^\circ$ . Note that this trajectory is based on the center of the load-end of the shuttle car. The three coordinates of the outer circle can be determined as shown below. (Coordinates are in centimeters.)

$$\begin{aligned}
x_1 &= 0.0 & y_1 &= 72.5 \text{ (Half the length of the shuttle car)} \\
x_2 &= 0.0 + L(\sin(-12.0^\circ)) = -11.4 & y_2 &= 72.5 + L(\cos(-12.0^\circ)) = 126.3 \\
x_3 &= x_2 = -11.4 & y_3 &= -y_2 = -126.3
\end{aligned}$$

Recall the equation of a circle, shown below.

$$x^2 + y^2 + 2ax + 2by + c = 0 \quad (5.1)$$

Because all three points belong to one circle, the following system of equations can be written.

$$x_1^2 + y_1^2 + 2ax_1 + 2by_1 + c = 0 \quad (5.2)$$

$$x_2^2 + y_2^2 + 2ax_2 + 2by_2 + c = 0 \quad (5.3)$$

$$x_3^2 + y_3^2 + 2ax_3 + 2by_3 + c = 0 \quad (5.4)$$

This gives three equations with three unknowns:  $a$ ,  $b$ , and  $c$ . These equations can be rearranged as shown below to solve for  $a$ ,  $b$ , and  $c$ .

$$\begin{bmatrix} 2x_1 & 2y_1 & 1 \\ 2x_2 & 2y_2 & 1 \\ 2x_3 & 2y_3 & 1 \end{bmatrix} \begin{bmatrix} a \\ b \\ c \end{bmatrix} = \begin{bmatrix} -(x_1^2 + y_1^2) \\ -(x_2^2 + y_2^2) \\ -(x_3^2 + y_3^2) \end{bmatrix} \quad (5.5)$$

The coordinates of the center of the circle,  $x_c$  and  $y_c$ , and the radius,  $R_2$  are determined as:

$$x_c = -a \quad (5.6)$$

$$y_c = -b \quad (5.7)$$

$$R_2 = \sqrt{x_c^2 + y_c^2 - c} \quad (5.8)$$

Solving this system of equations gives,

$$x_c = -473.4, \quad y_c = 0, \quad R_2 = 478.9$$

From this result, the radius of the circle that the center of the shuttle car follows is 473.4 cm and the radius of the circle that the load-end of the shuttle car follows is 478.9 cm. The arc length,  $s$ , Equation 5.9, from the starting point to the waypoint is used to determine the distance needed to tram the shuttle car. The final pose of the shuttle car will be approximately tangent to the inner circle that the center of the shuttle car follows, shown in Figure 5.1.

$$s = R_1\theta_2 \quad (5.9)$$

### 5.2.2 Steering Commands

PWM signals are a technique to represent an analog signal as a digital signal. Analog signals (continuous-time signals that have variable voltages) are turned into digital signals (discrete signals that are either on or off) by controlling the timing of how long they are on.

The shuttle car steering servomotors use standard PWM signals for steering control. The pulse length ranges from 1000  $\mu\text{s}$  to 2000  $\mu\text{s}$ . A pulse length of 1500  $\mu\text{s}$  corresponds to the neutral position of the servomotor, while pulse lengths of 1000 and 2000  $\mu\text{s}$  correspond to the maximum rotation counterclockwise and clockwise, respectively.

The radius and distance mentioned above are converted into signals that are decoded by an Arduino Uno. Accepting angle signals of  $0^\circ$  to  $180^\circ$ , the Arduino decodes the given signals into PWM signals. However, due to limitations in the steering linkage, the servo motors are limited from  $40^\circ$  to  $140^\circ$  (1222  $\mu\text{s}$  to 1778  $\mu\text{s}$ , in terms of pulse lengths), with a straight angle of  $87^\circ$  for the load-end axle and  $89^\circ$  for the discharge-end axle. Ideally, a signal corresponding to  $90^\circ$  for each axle would be used, but there was a

slight misalignment when connecting the servomotor horns to the inner tie rods. Tests were conducted to determine the turning radius for various angle signals, displayed in Table 5.1.

Table 5.1 Turning Radius Data

Angle Signal	Turn Radius, cm
40	60.5
42	62.5
44	64.5
46	69.0
48	71.5
50	75.0
52	78.5
54	82.5
56	87.5
58	93.5
60	99.5
61	104.5
62	108.0
64	115.5
66	125.5
68	138.0
70	153.0
72	170.0
74	194.0
76	226.0
78	270.0
80	337.0
82	353.8 (calculated)
84	445.6 (calculated)
86	608.8 (calculated)
87	742.5 (calculated)

Because of the limitations in the area available for measuring turning radii, the largest radius that could be established by testing was 337 cm, corresponding to a signal of 80 (see Figure 5.2). The remainder of the calculations were based on standard formulas for four-wheel steering based on the angle of the wheel for signals 82-87. It was extremely difficult to measure these angles, so several experiments were conducted using shorter

segments of circles to develop the best estimates of the turn radius for angle signals greater than 80.

Although the plot (see Figure 5.2) of controller signal vs turn radius was very well-behaved, a single polynomial could not be used to describe this relationship. Therefore, it was determined that the best-fit trend line for these values were piecewise third-order polynomials. Figures 5.3 through 5.6 show the graphs of the turning radius data with their trend line equations.

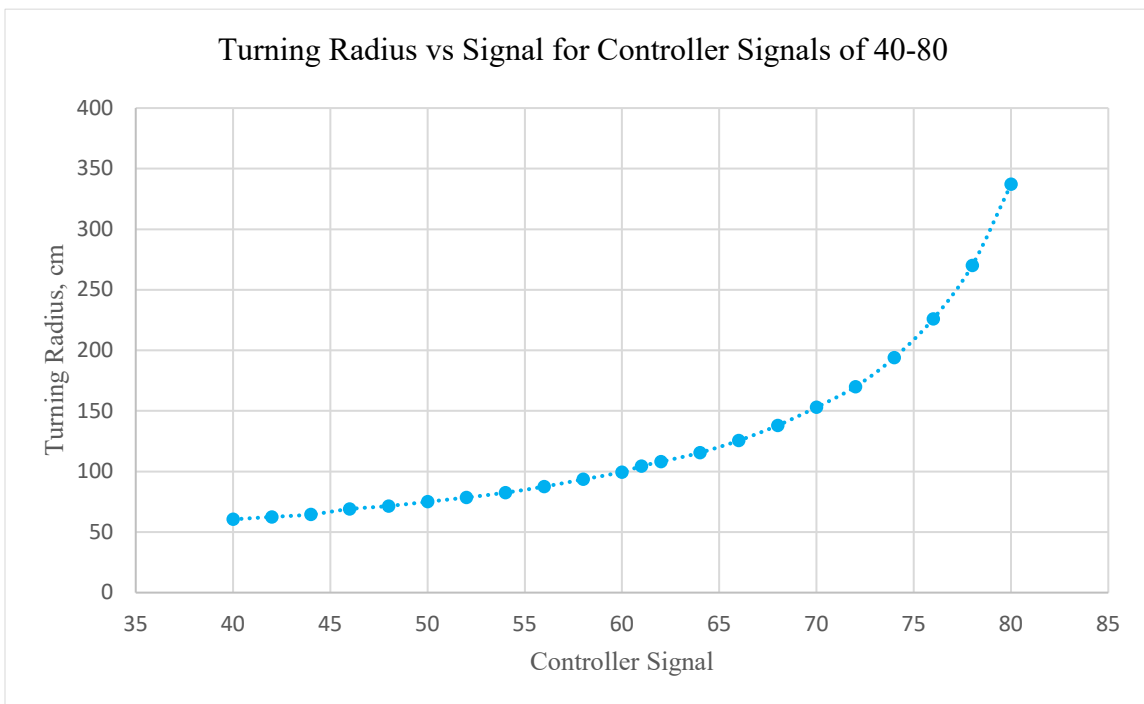


Figure 5.2 Plot of Measured Turning Radii for Controller Signals Ranging from 40 to 80

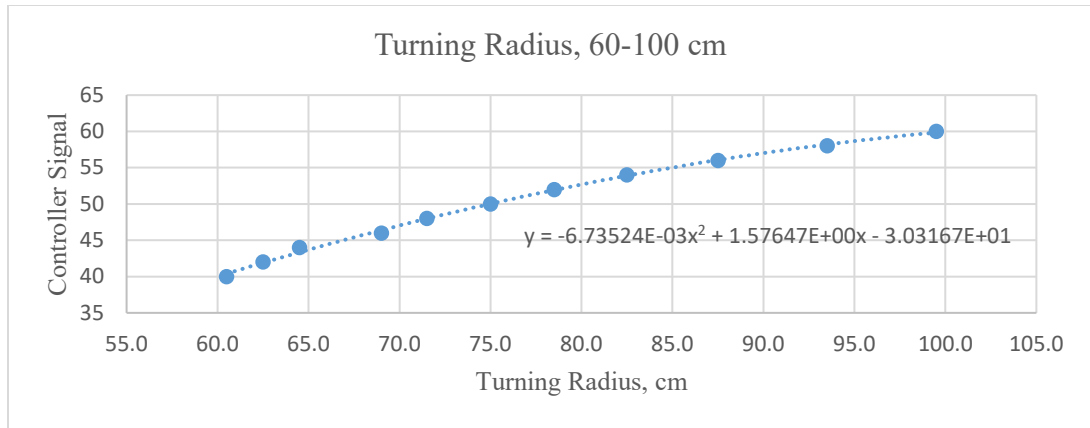


Figure 5.3 Plotted Turning Radius Data at Range of 60-100cm

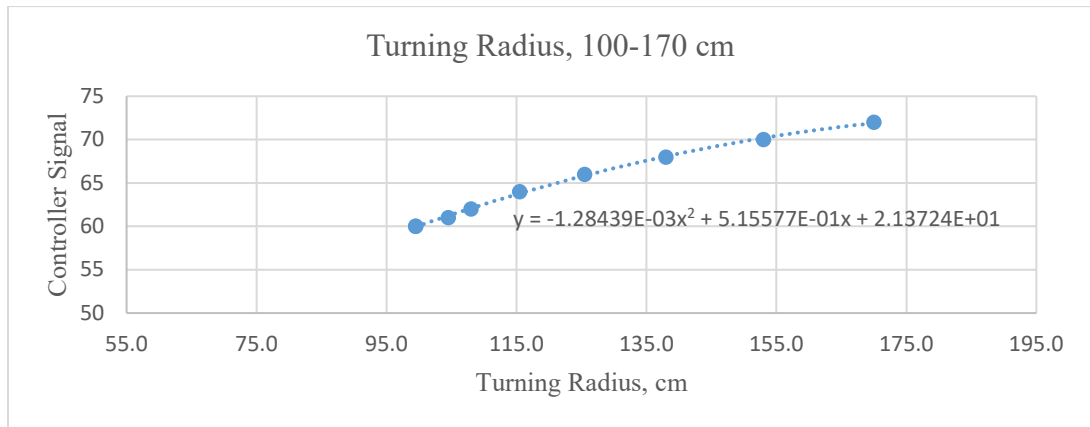


Figure 5.4 Plotted Turning Radius Data at Range of 100-170cm

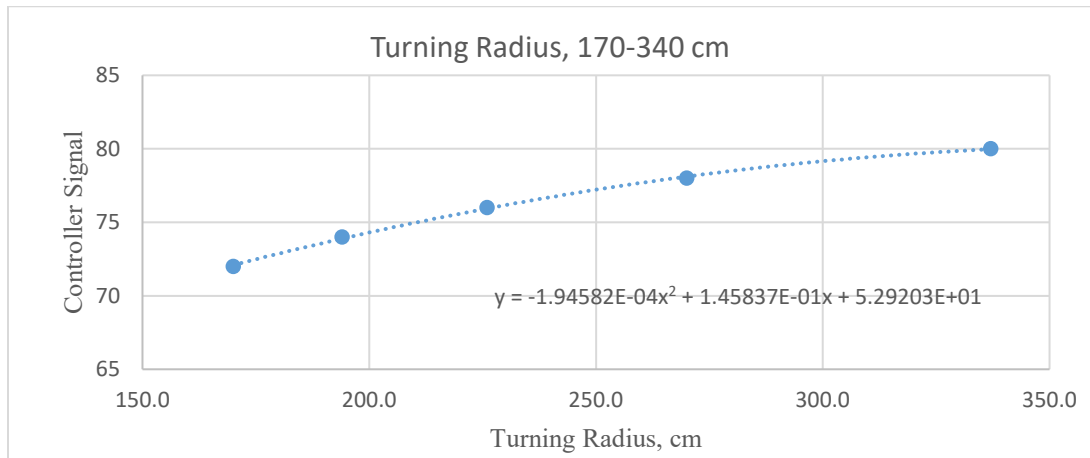


Figure 5.5 Plotted Turning Radius Data at Range of 170-340cm

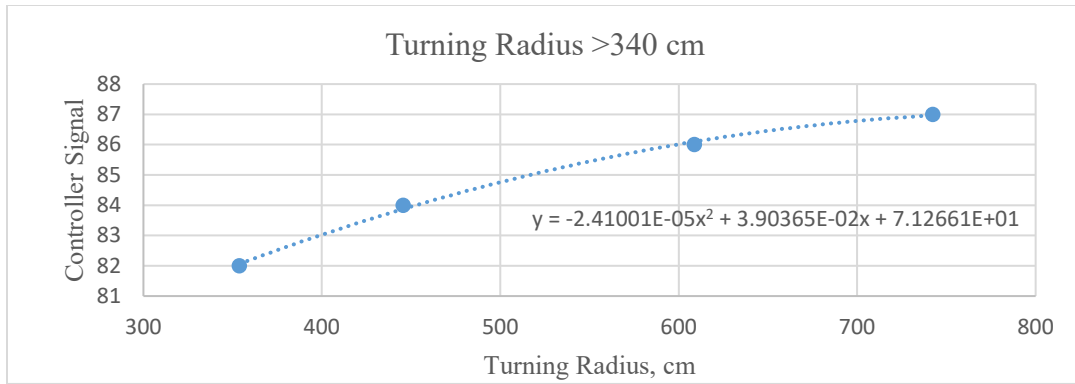


Figure 5.6 Plotted Turning Radius Data at Range of Greater than 340cm

Each test was done while the shuttle car was turning to the left. Due to the shuttle car mirroring the turns and the piecewise equations, it was not necessary to repeat the turning radius collection when turning to the right. Figure 5.7 shows the trend lines graphed, with the original trend lines at the bottom and the mirrored trend lines at the top.

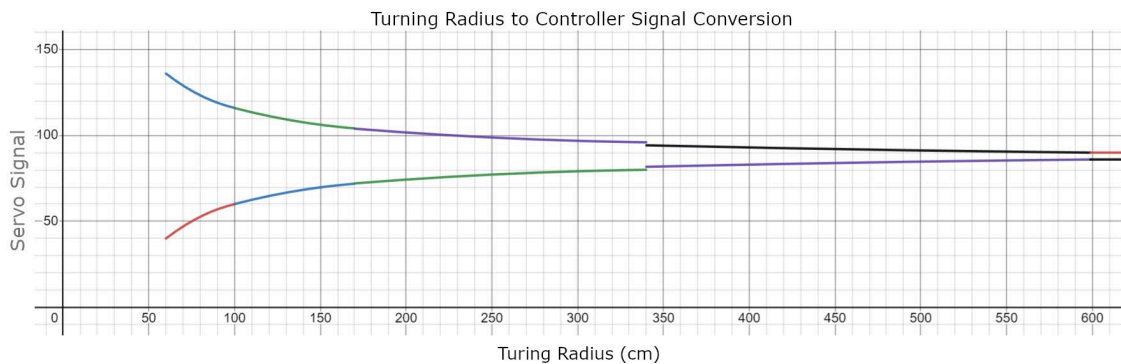


Figure 5.7 Mirrored Trend Lines

### 5.2.3 Navigation Algorithm Performance

The original algorithm planned by SRI (see Figure 3.9) included estimation of the pose of the continuous miner tail to be used to attempt to align the shuttle car with the CM tail. However, there were difficulties with this process and in most cases, it would not be possible to align the shuttle car with the CM tail because of space constraints; consequently, the pose estimation was eliminated from the pipeline. Instead, the path

planner was developed to center the shuttle car under the center of the conveyor tail. In addition, the new model combined both the original detection network and segmentation network. This improved the overall efficiency of the pipeline, because only one network (the new segmentation model) is required for the detection and segmentation capabilities provided from two networks in the original pipeline. An updated visualization of the navigation algorithm is displayed in Figure 5.8.

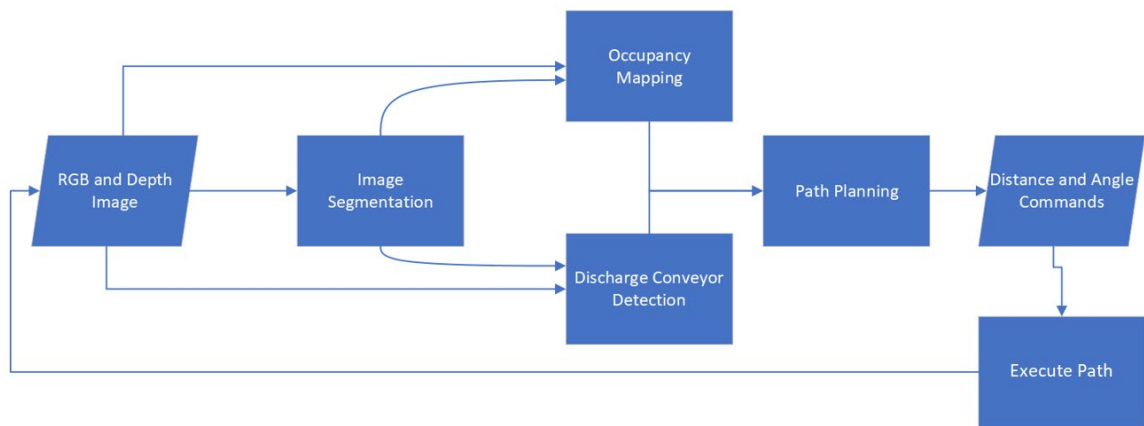


Figure 5.8 Block Diagram of the Final Autonomous Navigation Algorithm

### 5.3 Lab-Scale Assessment

Lab-scale testing began in March 2022 and continued until April 2023. Preliminary testing was conducted from March to September 2022 and was used to refine the pipeline. Evaluation testing began in October 2022. Results of the first series of evaluation testing are presented in Table 5.2. The information presented in Table 5.2 include the following:

Column 1 identifies the test number.

Column 2 is the distance from the target (in cm), i.e., the CM conveyor tail, to the sensor mounted on the shuttle car (SC) at the start of the test.

Column 3 is the distance from the target (in cm), i.e., the CM conveyor tail, to the sensor mounted on the shuttle car at the end of the test. Note that the ideal end distance ranges from approximately 35 cm to 45 cm, although this depends somewhat on the orientation of the continuous miner and shuttle car.

Column 4 provides summary remarks of the test.

Table 5.2 Results of First Series of Tests

Test	Start Distance from Camera, cm	End Distance from Camera, cm	Comments
1	-	-	Offline Pipeline to test update
2	-	-	Preliminary test of live pipeline
3	287	23	Start: Centered End: SC centered under conveyor tail, slightly closer than ideal
4	302	46	Start: Left rib End: Good distance, little too far left
5	305	46	Start: Left rib End: Good distance, little too far left (OK)
6	284	25	Start: Left rib End: Good distance, centered (OK)
7	284	25	Start: Right rib End: Little close, centered (OK)
8	287	58	Start: Right rib End: Good distance, centered (OK)
9	287	36	Start: Center, angled to the left End: Good distance, centered (OK)
10	292	64	Start: Centered, angled to the right End: SC on good path, but the pipeline stopped.
11	287	58	Start: Centered, angled to the right End: Centered, a little short (OK)

Test	Start Distance from Camera, cm	End Distance from Camera, cm	Comments
12	297	84	Start: Centered, with person in path End: SC on track to target, but stopped because of person
13	297	36	Start: Left rib, with person to the left of target End: SC docked with target, and avoided person (OK)
14	305	-	Start: Right rib, but angled slightly to the left, with person in path End: hit person
15	300	56	Start: Centered, with person in path End: SC on track to target, hit person.

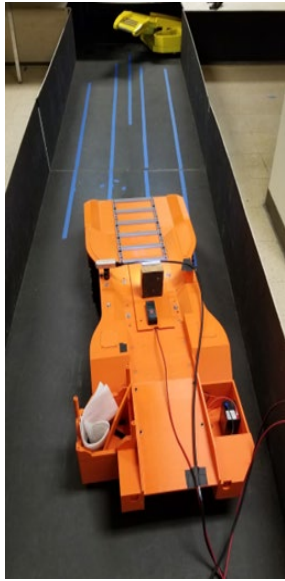
Table 5.3 shows the results of the second series of tests. Inspection of this table shows that the pipeline performed successfully in 12 of the 14 tests. In Test 11, the pipeline stopped because the shuttle car trammed too close to the rib and in Test 9, the shuttle car trammed to the right of the conveyor tail. Figure 5.9 shows a representative example of the start and end positions of the shuttle car (for Test 10 of the second series of tests). Blue masking tape can be seen in Figure 5.9, used as a navigation guide for testing in Section 5.2.

Table 5.3 Results of Second Series of October Tests

Test	Start Distance from Camera, cm	End Distance from Camera, cm	Comments
1	287	33	Start: Shuttle car near left rib. End: Good distance, centered
2	294	35	Start: Left rib, angled right End: Good distance, SC under target

Test	Start Distance from Camera, cm	End Distance from Camera, cm	Comments
3	292	33	Start: Left rib, angled right. End: Good distance, SC under target
4	292	35	Start: Centered End: Good distance, SC under target
5	297	38	Start: Centered, angled left End: Good distance, SC under target
6	284	45	Start: Centered, angled left. End: Good distance, SC under target
7	302	45	Start: Left rib End: Good distance, SC under target
8	289	40	Start: Left rib, angled right End: Good distance, SC under target
9	294	35	Start: Right rib, angled left End: Good distance, right of target. Loose wheel found, tightened
10	297	38	Start: Right rib, angled left End: Good distance, SC under target
11	289	127	Start: Left rib, angled right End: Pipeline stopped because SC trammed too close to right rib
12	292	40	Start: Left rib, angled right End: Good distance, SC under target
13	290	41	Start: Centered, angled left End: Good distance, shuttle car under target

Test	Start Distance from Camera, cm	End Distance from Camera, cm	Comments
14	295	38	Start: Right rib, angled slightly right End: Good distance, shuttle car under target



(a) Starting Position



(b) Ending Position

Figure 5.9 Start and End Positions of Shuttle Car for Test 10 of Table 5.3

Following those tests, several refinements were made to the pipeline. One included adding the capability of the pipeline to send a backup signal to the shuttle car in cases where the continuous miner backs up while the shuttle car is positioned under the tail, or if the shuttle car trams closer than the planned distance. Another improvement included the ability to establish unique detection thresholds for each class of the following objects: person, rib, CM body, CM tail, mine floor, mine ceiling, and shuttle car body. A series of tests were conducted in April 2023 to specifically address these changes and are presented in Table 5.4.

Table 5.4 Summary of Final Lab-Scale Tests

Test	Start Distance from Camera, cm	End Distance from Camera, cm	Comments
1	178	41	Start: SC left of center Conditions: No special conditions End: SC centered under conveyor tail
2	183	-	Start: SC centered, angled left Conditions: Person in path 132 cm from camera, <i>minInitDistFromPerson</i> set at 200 cm Response: Pipeline paused generating a path
3	183	41	Start: Same start conditions as test 2, but with person removed Response: SC trammed to distance less than <i>tooCloseThreshDist</i> then backed up to proper distance. End: SC centered under conveyor tail
4	183	41	Start: SC centered, angled right End: SC under conveyor tail, slightly right of center (requiring conveyor tail to be swung apx. 15° for ideal position)
5	201	28	Start: SC right of center, angled right End: SC under conveyor tail, right of center (requiring conveyor tail to be swung apx. 10° for ideal position) Final distance indicated by depth camera slightly less than measured

Test	Start Distance from Camera, cm	End Distance from Camera, cm	Comments
6	206	34	<p>Start: SC near right rib</p> <p>Response: SC trammed to distance less than <i>tooCloseThreshDist</i> then backed up to proper distance.</p> <p>End: SC under conveyor tail, right of center (requiring conveyor tail to be swung apx. 5° for ideal position)</p>

#### 5.4 Full-Scale Testing

Full-scale testing began after the second series of evaluation tests were completed. As explained in Chapter 3, the simulated mine lab at West Virginia’s Training and Conference Center was the location for full-scale testing.

As discussed in Chapter 4, the camera was positioned near the middle of the shuttle car on the offside. That position provided the best view of the continuous miner while preventing additional work and time on training the neural network from a new point of view. The camera was a ZED 2i stereo camera and was attached to a tripod. The tripod was then attached to the shuttle car via magnets.

Due to the time and cost required to build an interface and automatic controls on the shuttle car, the shuttle car was manually controlled. Therefore, when the algorithm gave a planned path, the algorithm was paused while a target was placed at the waypoint and the shuttle car was trammed via a human operator. Once the shuttle car was stopped and at the waypoint determined by the path planning, the algorithm was resumed.

#### 5.4.1 Full-Scale Testing

When the full-scale testing began, it was noticed that the shuttle car axles were not correctly aligned, causing the shuttle car to slightly veer to the left. Fortunately, the operator quickly learned how to compensate for this and was able to tram the shuttle car to the waypoint given by the algorithm. Also, the shuttle car had one broken headlight and one headlight that was very dim, so two external headlights were added above the existing headlights, as shown in Figure 5.10.



Figure 5.10 Externally Mounted Headlight to Shuttle Car Load-End

Several issues with the pipeline were addressed during full-scale testing. For example, because the external headlights were mounted on top of the shuttle car, they were sometimes misclassified as a person. This is shown in Figure 5.11 as the red blob, and in the RGB image, Figure 5.12.



Figure 5.11 Segmented Image of Misclassified Headlight



Figure 5.12 RGB Image of Headlight

The algorithm would sometimes misclassify ventilation curtains. The reflection caused by the headlights would sometimes cause the algorithm to classify the curtain as a person, causing the pipeline to stop giving planned paths. An example is shown in Figure 5.13 as the left-most red blob, and in the RGB image, Figure 5.14. Modifications were made to the algorithm to adjust detection thresholds and classify these objects as noise and ignore them.



Figure 5.13 Segmented Image of Curtain



Figure 5.14 RGB Image of Curtain

There were a couple of instances where the algorithm would detect that a person (or an object) was in the path of the shuttle car. However, it would ignore the person and plan a path. This is shown in Figure 5.15 as the right-most red blob, with the RGB image in Figure 5.16. Figure 5.17 shows the planned path that the algorithm generated.

To address this, changes were made in the detection threshold for people. A parameter was also added to allow the user to define a distinct minimum distance to

increase the clearance for people compared with other obstacles. This parameter causes the algorithm to pause until the person is either beyond the minimum distance or out of view, correcting the abovementioned issues.



Figure 5.15 Segmented Image of Person in Shuttle Car Path



Figure 5.16 RGB Image of Person in Shuttle Car Path

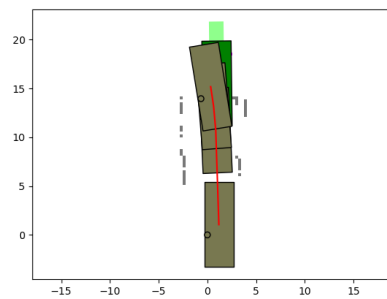


Figure 5.17 Incorrectly Planned Path with a Person in Shuttle Car Path

A few situations occurred where the algorithm planned a path well beyond the target. A modification was made to add a user-defined parameter that would limit the maximum distance beyond the target for which a path would be accepted. This parameter caused the algorithm to reject paths beyond the distance defined by the user, and eliminated the issue.

The appendix provides a summary of tests conducted from November 2022 through February 2023.

#### 5.4.2 Full-Scale Final Assessment

Once the issues with the algorithm were addressed, the algorithm planned paths consistently and accurately. A representative example is shown in Figures 5.18 and 5.19 for a situation in which the shuttle car start point was approximately 21.6 meters away from the continuous miner. The shuttle car was trammed to the continuous miner, in four planned paths, and was positioned correctly under the discharge conveyor (Figure 5.19).



Figure 5.18 Starting Position of Representative Full-Scale Test

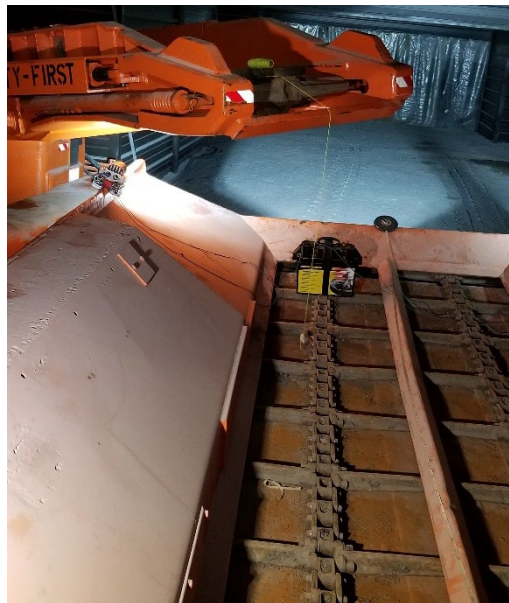


Figure 5.19 Ending Position of Representative Full-Scale Test

Table 5.5 summarizes the equipment's starting locations and distances and the results of the tests for the final set of tests conducted in April 2023. The ending position of the shuttle car would sometimes be slightly to the left or right of the center of the continuous miner tail. However, this is not a serious issue because the continuous miner operator could swing the discharge conveyor several degrees to center it above the shuttle car.

Table 5.5 Full-Scale Results Summary

Test	Start Distance, m	End Distance, m	Comments
1	30.4	3.5	CM: In right crosscut Start: Left rib, angled left End: SC under CM conveyor tail, slightly left of center
2	18.9	3.3	CM: In right crosscut Start: Right rib, angled right End: Centered under conveyor tail
3	20.4	4.3	CM: In right crosscut Start: Right rib, angled right End: SC centered under conveyor tail
4	21.4	3.5	CM: In left crosscut Start: Right rib, angled right Observations: At waypoint 2, the path planner planned a path that exceeded the practical limit for the shuttle car. This path was ignored and the pipeline subsequently produced a valid path. End: SC centered under conveyor tail.

Test	Start Distance, m	End Distance, m	Comments
5	22.3	-	<p>CM: In left crosscut</p> <p>Start: Left rib, angled left</p> <p>Observation: At waypoint 2, the path planner planned a path that was too far to the left for proper coal loading.</p> <p>End: Too far left for practical loading</p>
6	21.6	2.8	<p>CM: In left crosscut</p> <p>Start: Right rib, angled right</p> <p>End: SC under the conveyor tail, slightly right of center</p>
7	22.3	3.1	<p>CM: In left crosscut</p> <p>Start: Right rib, centered</p> <p>End: Under CM conveyor tail, slightly right of center</p>

## CHAPTER 6. PATH PLANNING

### 6.1 Introduction

As stated in Chapter 5, the autonomous navigation system will plan a path when the continuous miner is detected, and the occupancy map is created. Two methods were integrated into the navigation system to plan a path to the continuous miner. Rapidly exploring random trees sharp (RRT#) and transition-based rapidly exploring random trees (TRRT). These methods are different versions of the same base algorithm, RRT, as described in Section 2.1.2.

### 6.2 Implemented Algorithm Comparison

As explained in Chapter 2, RRT will first pick a random node between the starting node and a node up to a user-defined maximum distance. It checks the location of the random node and compares if the node is within the bounds of an obstacle. It will connect the node with its nearest neighboring node unless the node is in the bounds of an obstacle, in which case, the node will be ignored. To confirm completion, RRT will check if the current node is within the bounds of the target [6]. The randomization of the nodes with their nearest neighbor is the cause of its name, as displayed in Figure 6.1.

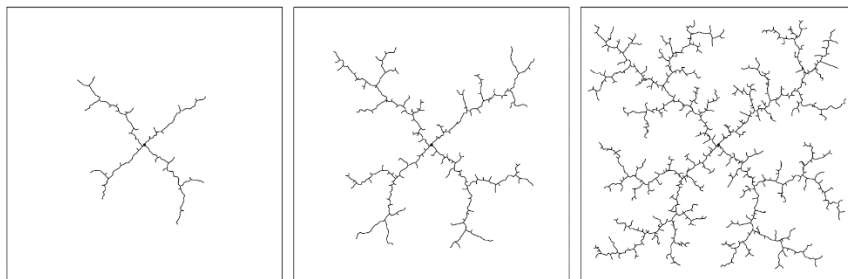


Figure 6.1 Rapidly Exploring Random Trees [12]

RRT# is a variant of the base algorithm, RRT. RRT# behaves the same as RRT; however, with one exception: information about the lowest cost path (the shortest distance between nodes) is stored. This produces better efficiency as the range of nodes to search is narrower [7]. In lab-scale testing, this method often took more than five seconds to generate a path.

TRRT is the other variant of RRT. TRRT assigns states to nodes and accepts them, or ignores them, based on the ease of navigation from their nearest neighbors. This approach does not create an optimal path to the continuous miner; however, it creates a path more quickly than RRT [8]. During lab-scale testing, this method generally took less than a second to generate a path.

Due to the low computational time, it would be inferred that TRRT would be the preferred method to use. However, in lab-scale testing, it was found that TRRT would create many short steps in its generated path. This is illustrated in Figure 6.2, with the left image (a) showing the TRRT method and the right image (b) showing the RRT# method. Clearly, the path planned by TRRT would not be an acceptable path because of the time it would take to execute a large number of steps. Therefore, in both lab-scale and full-scale, the RRT# method was used for path planning.

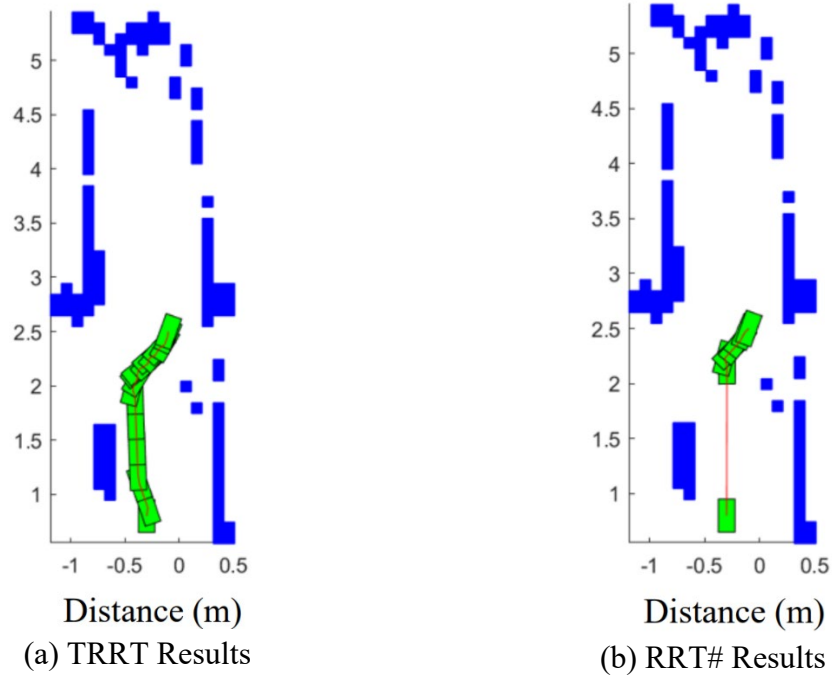


Figure 6.2 Representative Comparison of Path Planning Methods

An issue with using RRT# is its long computational time. If the autonomous navigation system were to be used in industrial applications, path planning would need to be fast to react to dynamic situations in mining.

### 6.3 A\* Algorithm Development

Because of the long computation time of RRT#, the final aspect of this research involved the investigation and development of an alternative path planner that would execute quickly and general valid paths. After investigating several path planning algorithms, it was decided to use A\*. Explained in Chapter 2, A\* is a popular path-searching algorithm because of its ability to find the shortest paths efficiently. Due to its simplicity, the coordinates of the starting point and the target are given to A\* at the start. Beginning at the start node, A\* finds a neighboring node with the smallest cost (estimated

shortest distance or time from a heuristic function) and connects them. A\* can connect to neighboring nodes in four directions (0°, 90°, 180°, 270°) or eight directions (0°, 45°...), the mode of movement depends on the choice of the user. It iterates this process and connects the neighboring nodes until the current node is the target [10].

When comparing the computational speed of A\* to RRT, and its variants, A\* was found to be the fastest method to plan a path to the continuous miner. An investigation was done comparing A\* and RRT\* by Braun, et al. [28]. They observed, in different scenarios, that RRT\* was magnitudes of order slower than A\* in terms of computational speed.

When comparing the generated path of A\* to RRT, and its variants, there is little variation among the resulting generated paths. A representative comparison is shown in Figure 6.3, which displays the RRT# result, and Figure 6.4, which displays the A\* result. Figure 6.3, the RRT# result, generates three waypoints to the goal. Figure 6.4, the A\* result, generates two waypoints to the goal. Comparison of other paths confirmed that A\* has relatively the same path planning result as RRT# for this application.

Because A\* could not be implemented into the main autonomous navigation system (source code was not available), an external program was developed to compare the differences. The program used parts of source code from another program that was hosted on GitHub [29]. The input for the A\* path planner is the occupancy map.

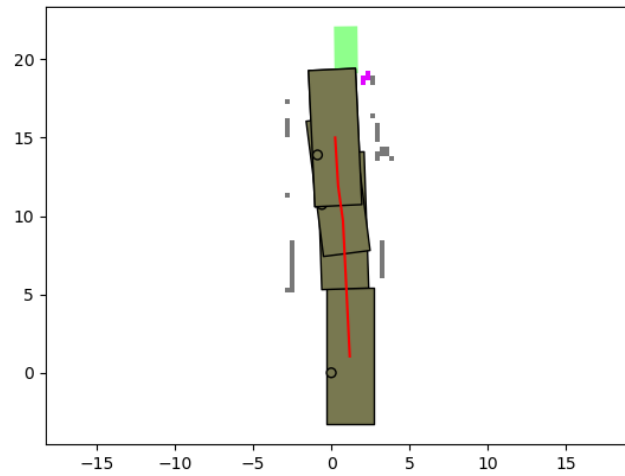


Figure 6.3 RRT# Path Planning Result

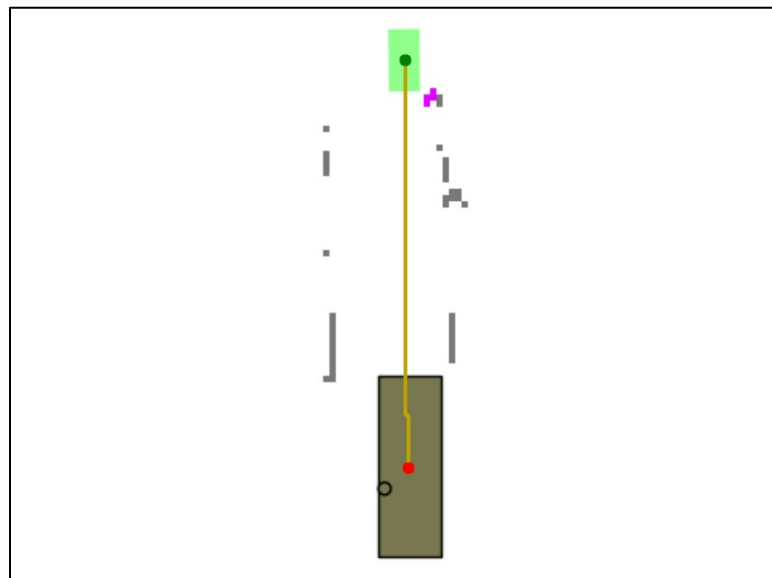


Figure 6.4 A\* Path Planning Result

The A\* path planner generated a valid path in less than half a second. This execution speed is much faster than the time for RRT# (over five seconds). Based on the potential for the use of A\* to reduce the path planning time by an order of magnitude, it was decided to develop an A\* path planner for the lab-scale controller.

However, even with all these benefits, the A\* path planner has some serious limitations for this application. One limitation is that A\* does not consider the dimensions of the vehicle, i.e., the shuttle car is considered to be the size of a single pixel. The result of this was that the algorithm planned paths for the centroid of the shuttle car and did not consider the clearances required for the shuttle car body to navigate around objects without hitting them. An example of this is shown in Figure 6.5 for an obstacle in the center of the entry. Although it is impossible for the shuttle car to follow this path because its width is approximately one-half of the entry width, a path is generated.

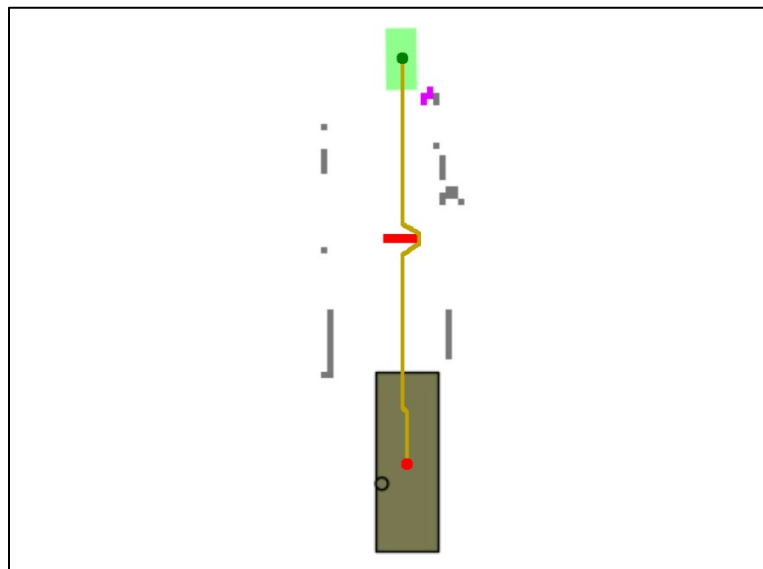


Figure 6.5 A\* Bad Path Result

To address this issue, a simple modification was made to the A\* algorithm. The modification involved adding a smoothing function that changed the costs of nodes based on how far they are from the obstacle. This function removes hard edges between nodes by equally spacing nodes, giving a smoother dataset [31]. This allowed the algorithm to adjust the path based on the dimensions of the shuttle car and obstacles. Figure 6.6 shows

the result of the same situation with the modified path planner to compensate for shuttle car dimensions.

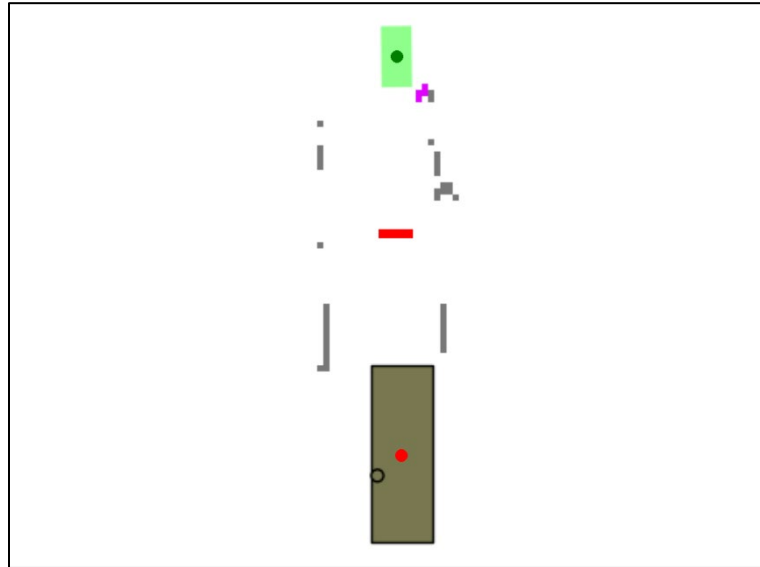


Figure 6.6 A\* No Path

After this modification, additional testing was conducted with the shuttle car and obstacles at different locations. During this phase of testing, it was determined that the smoothing function failed to plan valid paths around obstacles. Based on these results, the smoothing function was removed from the path planner. To account for the dimensions of the shuttle car, it was decided to modify the occupancy map to account for the shuttle car dimensions before the A\* algorithm was applied. This modification allowed the start, goal, and obstacle to be automatically detected and the width to be automatically calculated, displayed as the original map in Figure 6.7 and the modified map in Figure 6.8.



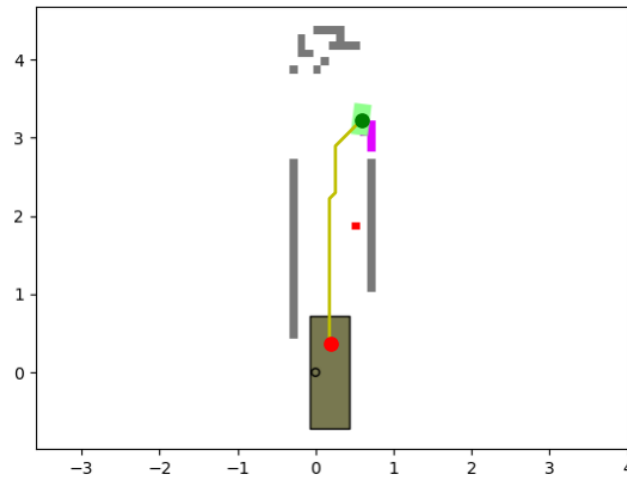


Figure 6.9 Path Avoiding Obstacle

As previously described, a separate program had to be used to test the A\* algorithm using only the occupancy grid map output of the automated navigation algorithm. In addition, the navigation algorithm is proprietary and other data is inaccessible (i.e., raw depth information). Therefore, distance had to be calculated using only the occupancy grid map image.

Unfortunately, an issue is that the size of the pixels in the occupancy grid map change based on the point of view of the camera and how far the shuttle car is from the miner, preventing consistency in calculating distance from the coordinate system. A solution was to use the known width of the mock mine entry, giving a known distance. The number of pixels between the ribs in the occupancy grid map then could be measured. Dividing the entry width by number of pixels gives a scale to calculate dimensions of a pixel.

Unfortunately, this modification failed to provide accurate distances for the path planner. An example of this is shown in Figure 6.10 and Figure 6.11. Figure 6.10 shows

the shuttle car docked correctly and Figure 6.11 shows the shuttle car short of the miner conveyor tail, only having a slightly different starting position between the two.



Figure 6.10 Shuttle Car Docked Correctly Under Miner Conveyor



Figure 6.11 Shuttle Car Incorrectly Docked, Short of Conveyor

To address this issue, it was decided to use the measured distance from the shuttle car load-end to the middle of the conveyor, rather than the width of the mine. Therefore, the actual distance was used to establish the pixel dimensions. Unfortunately, this method requires manual intervention. However, this is not considered an issue, because the depth information from the RGBD camera would ordinarily be available to the path planner. Preliminary test results with this modification were successful, so final testing was conducted, described in the next section.

#### 6.4 A\* Results

For evaluation of the A\* path planner, three shuttle car start positions, three continuous miner start positions, and one obstacle position were used. A visualization of the mock mine, continuous miner start position, shuttle car start position, and obstacle

location are shown in Figure 6.12. Table 6.1 shows results of the combinations shown in Figure 6.12.

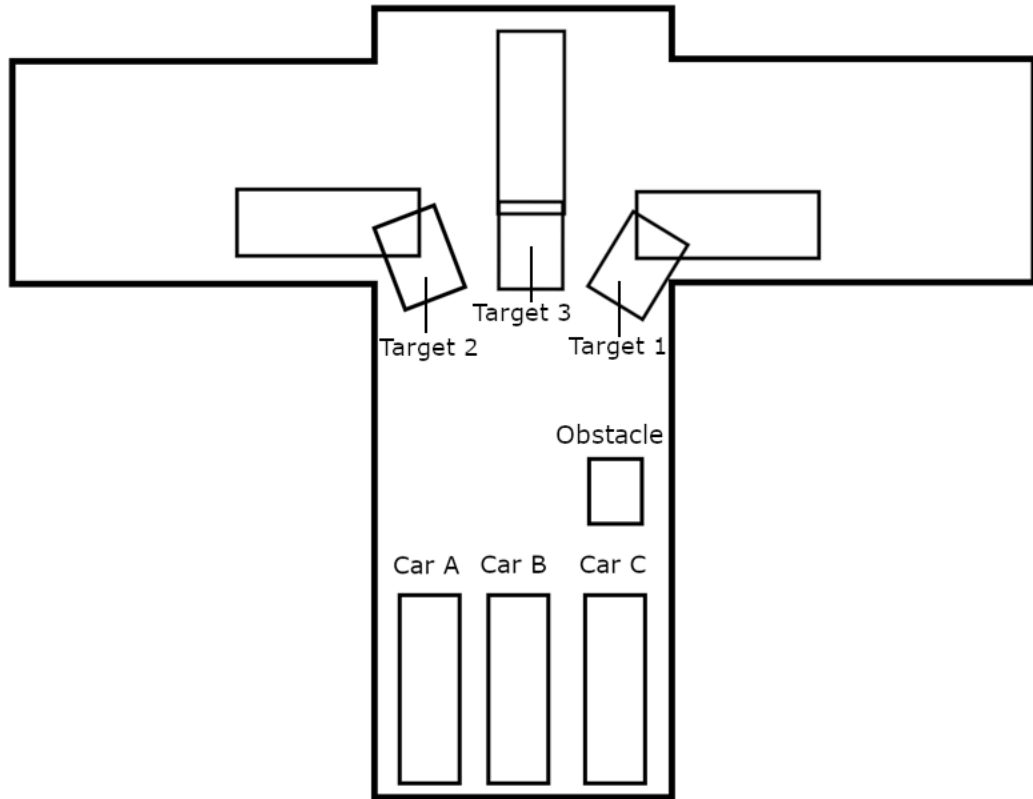


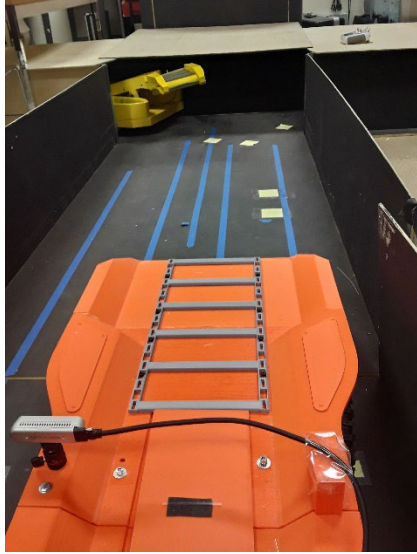
Figure 6.12 Position of CM, Obstacle, and Shuttle Car Start Position for A\* Path Planner Evaluation

Table 6.1 A\* Evaluation Results Summary

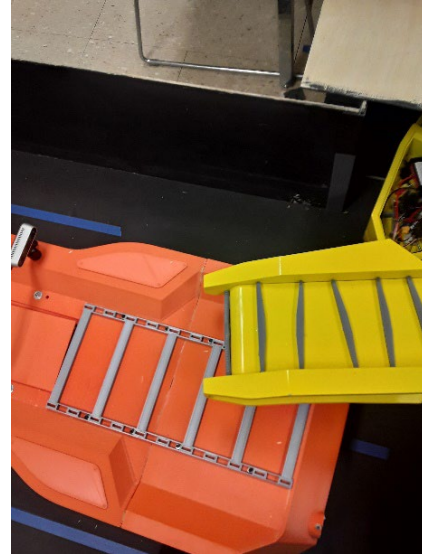
Test	Starting Location	Miner Location	Obstacle?	Starting Distance, cm	Comments
1	A	1	Yes	180	Good distance, left of conveyor
2	B	1	Yes	183	Good distance, slightly left of conveyor
3	C	1	No	180	Good distance, slightly right of conveyor
4	A	2	No	175	Good distance, slightly left of conveyor

Test	Starting Location	Miner Location	Obstacle?	Starting Distance, cm	Comments
5	B	2	No	178	Good distance, slightly right of conveyor
6	C	2	No	175	Good distance, slightly right of conveyor
7	C	2	Yes	175	Good distance, slightly left of conveyor
8	A	3	No	163	Good distance, centered
9	B	3	No	165	Good distance, centered
10	C	3	No	163	Good distance, centered

Inspection of Table 6.1 shows that the A\* algorithm performed successfully in all 10 tests. In Test 1, the test that performed that worst, the shuttle car's final position was at the correct distance, but left of the conveyor. The continuous miner operator could correct this error by swinging the conveyor. Figure 6.13 shows the success of the A\* algorithm with the start and end positions of the shuttle car from Test 6 in Table 6.1. As mentioned in Chapter 5, blue masking tape can be seen in Figure 6.13 and was used as a frame of reference for various trajectories. Post-it notes can also be seen in Figure 6.13, being used as landmarks for the continuous miner and obstacle placement.



(a) Start Position



(b) End Position

Figure 6.13 Start and End Positions of Shuttle Car for Test 6 of Table 6.1

## CHAPTER 7. CONCLUSION

### 7.1 Research Conclusion

Accurate and reliable autonomous navigation is difficult without GPS, because vehicle location cannot be continuously updated by triangulation. This problem is exacerbated underground with rough terrain, confined roof heights, and low lighting. For a shuttle car to approach the continuous miner, the navigation system needs to have the ability to determine the continuous miner conveyor tail location and plan a path to it. The planned path must also avoid obstacles. This research showed that the navigation pipeline, shown in Figure 7.1 could autonomously navigate a shuttle car to a continuous miner using RGBD imagery, semantic segmentation, occupancy mapping, path planning, and path execution.

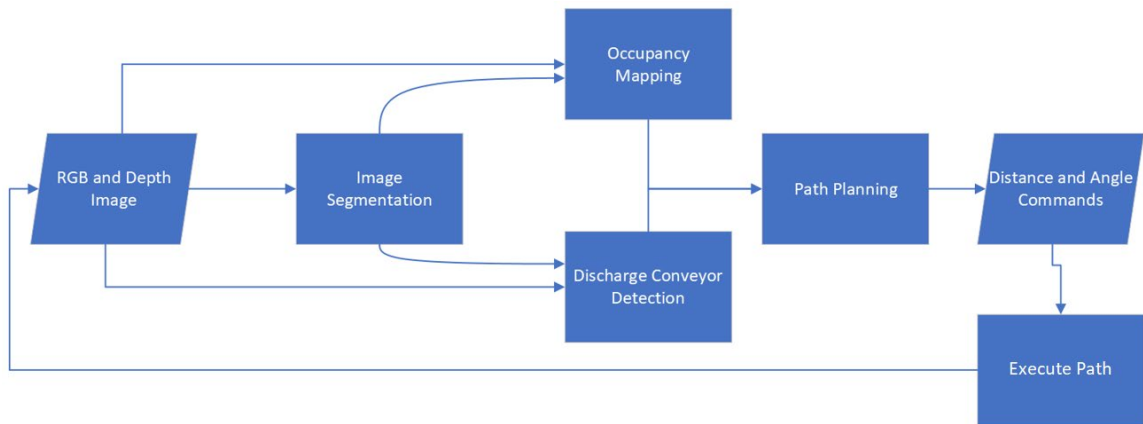


Figure 7.1 Block Diagram of Autonomous Navigation Pipeline

Over 400 images were taken at various distances and angles between the shuttle car and the continuous miner to train the image segmentation process. The images were annotated with the shuttle car and the continuous miner as the focus. This allowed for a more basic segmentation of obstacles because the algorithm would only need to recognize the distance between the shuttle car, obstacles, and the continuous miner. However, this

eventually caused problems with external headlights and ventilation curtains being segmented and labeled as people. This was corrected by adjusting detection thresholds that the caused the algorithm to identify them as noise and correctly plan a path to the continuous miner conveyor tail.

## 7.2 Future Work

Several areas of work have been identified to be helpful in the future. These include attaching additional sensors to the shuttle car, modifying the path planning algorithm, further refining and integrating the navigation system into a single program, and developing autonomous controls to navigate a full-scale shuttle car.

This approach has been shown to be feasible; however, using a single RGB-Depth camera as the sensor may not be reliable in certain circumstances, e.g., when mine personal approach the side of the shuttle car out of the camera field of view. Therefore, attaching additional sensors to the shuttle car would be beneficial for avoiding miners, other mining equipment, and other obstacles. For example, using LiDAR sensors would allow for redundancy checks with the RGB-Depth camera. The camera also captures orientation and acceleration data that was not used in this work, using this data could be another redundancy check.

During this research, there were no opportunities to collect data at an operating mine. Future work should include collection of images in operating coal mines under various conditions.

The A\* path planner was significantly faster than RRT# and planned paths that were very similar to those developed by RRT# from both algorithms were relatively the

same. Therefore, additional research into the implementation of A\* should be conducted. However, several issues need to be addressed.

The A\* algorithm assumes that the vehicle, path, and target have dimensions of one pixel. Therefore, the algorithm does not provide the necessary clearances for avoiding obstacles. As described in Chapter 6, this could be compensated for by changing the length of the obstacle to at least the length of the shuttle car. Although this adjustment worked in the laboratory experiments, additional testing and development needs to be done.

Testing of the A\* path planner included only situations in which the start position of the shuttle car was approximately parallel with the entry. The current implementation of A\* does not account for shuttle car start positions that are angled with respect to the entries. The algorithm should be modified to work for any starting pose. (One method for addressing this issue would be to use the first waypoint to square the shuttle car in the entry and use subsequent images for path planning.)

Because the pipeline source code was not available, the A\* path planner could not be integrated into the autonomous navigation system. However, to be able to easily run and migrate the algorithm, it would need to be integrated into a single pipelined program for further evaluation.

Finally, there were insufficient resources available to add steering and tramping controls to the full-scale shuttle car. Future work should include these controls and an interface between the algorithm and the full-scale shuttle car controls.

APPENDIX

Table A Summary of November 2022 Full-Scale Testing

Test	Start Distance, m	End Distance, m	Min Step Size, m	Max Step Size, m	MinInit Dist, m	Comments
1	-	-	1.5	10.0	0.48	Start: Left rib End: SC centered under CM conveyor tail
2	28.0	-	1.5	10.0	0.48	Start: Right rib, angled left End: SC under CM conveyor tail, slightly left of center
3	-	-	1.5	10.0	0.48	Start: Centered, angled left End: SC under CM conveyor tail, slightly left of center
4	-	-	1.5	10.0	0.48	This is a test of person identification and avoidance. (Person 1.0 m from load-end of SC.) Start: Centered Outcome: Segmentation map clearly showed the person; however, a path was planned that would hit the person

Test	Start Distance, m	End Distance, m	Min Step Size, m	Max Step Size, m	MinInit Dist, m	Comments
5	-	-	1.5	10.0	0.48	This is a test of person identification. (Person 1.5 m from load-end of SC.) Start: Centered Outcome: Segmentation clearly showed the person; however, a path was planned that would hit the person
6	29.0	-	1.5	10.0	0.48	Start: Centered, angled left End position: SC under CM conveyor, slightly left of center
7	23.7	-	1.5	10.0	0.48	Start: Right rib End: Good trajectory until the last step; path planner approximately three meters too far

Table B Summary of December 2022 Full-Scale Testing

Test	Start Distance, m	End Distance, m	Min Step Size, m	Max Step Size, m	MinInit Dist, m	Comments
1	20.8	-	1.5	10.0	Target = 3 Person = 7	Start: SC centered, angled slightly left; CM turning right. End: SC under conveyor tail, slightly right of center
2	22.7	-	1.5	10.0	Target = 6 Person = 7	Start: Right rib; CM turning right. End: SC Centered under conveyor tail
3	22.6	5	1.5	10.0	Target = 6 Person = 12	Testing for avoiding person in path Start: Centered Person identified, pipeline paused until person moved from path, End: SC under conveyor tail, slightly left of center
4	30.9	4.4	1.5	10.0	Target = 6 Person = 12	Start: Right rib CM in straight At waypoint 2, the CM cable stand off was classified as a person; stand off was covered with small piece of ventilation curtain and pipeline resumed. End: Good distance, centered

Test	Start Distance, m	End Distance, m	Min Step Size, m	Max Step Size, m	MinInit Dist, m	Comments
5	28.3	-	1.5	10.0	Target = 6 Person = 12	Start: Centered, slightly angled left; CM in straight. At waypoint 1, the ventilation curtain was classified as a person. This was corrected by slightly adjusting the ventilation curtain. End: SC under conveyor tail, slightly left
6	24.7	4.21	1.5	10.0	Target = 4.5 Person = 12	Start: Left rib; CM in straight End: SC centered under conveyor tail

Table C Summary of January 2023 Full-Scale Testing

Test	Start Distance, m	End Distance, m	Min Step Size, m	Max Step Size, m	MinInit Dist, m	Comments
1	25.8	4	1.5	10.0	Target = 4.5 Person = 12	CM: In straight Start: Centered, angled slightly left. End: Under CM conveyor tail, slightly left of center
2	21.4	4.6	1.5	10.0	Target = 4.5 Person = 12	CM: In straight Start: Right rib End: Centered, under conveyor tail

Test	Start Distance, m	End Distance, m	Min Step Size, m	Max Step Size, m	MinInit Dist, m	Comments
3	18.3	-	1	10.0	Target = 4.5 Person = 12	Test of pipeline reacting to miner trammig forward CM: In straight Start: Left rib, angled right Reaction to CM trammig forward: After waypoint 3, SC was slightly left of conveyor tail at 4.3m. CM was then trammed forward (approx. 5 m) and pipeline produced 2 more waypoints to navigate the SC shuttle car to the conveyor tail. End: SC under conveyor tail, but left of center.
4	20.1	M: 3.4 P: 4.1	1.5	10.0	Target = 4.5 Person = 12	CM: In left crosscut Start: Left rib End: Under the conveyor tail, slightly right of center
5	21.9	M: 3.2 P: 3.8	1	10.0	Target = 4.5 Person = 12	CM: In left crosscut Start: Right rib, angled right End: Under the conveyor tail, slightly right of center

Test	Start Distance, m	End Distance, m	Min Step Size, m	Max Step Size, m	MinInit Dist, m	Comments
6	24	M: 4.4 P: 4.8	1	10.0	Target = 4.5 Person = 12	<p>Testing for correct behavior with person in path  CM: In left crosscut  Start: Centered  In all cases, pipeline reacted correctly to a person within <i>minInitDistFrom Person</i>.  Near the end of the test, a path was planned that would have directed the SC into, or very close to the rib, probably because of error in depth camera measuring distance to rib. That path was skipped, and a valid path was planned in the next step.  End: SC under conveyor tail, slightly left of center</p>

Test	Start Distance, m	End Distance, m	Min Step Size, m	Max Step Size, m	MinInit Dist, m	Comments
7	21.7	M: 3.5 P: 3.9	1	10.0	Target = 4.5 Person = 12	CM: In left crosscut Start: Centered, angled slightly left End: Centered under CM conveyor tail. Note: SC was within minInitDist for target distance, but generated a path
8	28.7	M: 4.1 P: 4.6	1	10.0	Target = 4.5 Person = 12	CM: In left crosscut Start: Centered, angled slightly left End: Centered under conveyor tail
9	28.1	4.5	1	10.0	Target = 4.5 Person = 12	CM: In straight Start: Right rib, angled slightly right End: SC centered under conveyor tail

Test	Start Distance, m	End Distance, m	Min Step Size, m	Max Step Size, m	MinInit Dist, m	Comments
10	22.4	4.4	1	10.0	Target = 5 Person = 12	<p>Testing for person in path CM: In straight Start: Left rib, angled left</p> <p>In all cases, pipeline reacted correctly to a person within <i>minInitDistFromPerson</i>.</p> <p>End: Centered under conveyor tail</p>

Table D Summary of February 2023 Full-Scale Testing

Test	Start Distance, m	End Distance, m	Min Step Size, m	Max Step Size, m	MinInit Dist, m	Comments
1	-	4.5	1.5	10.0	Target = 5 Person = 12	<p>Test of pipeline reacting to CM tramping backwards</p> <p>CM: In straight Start: Left rib, angled slightly left</p> <p>Reaction: The pipeline generated paths to the conveyor tail. Once positioned at that location, the CM was tramped backwards. The pipeline correctly generated a backup signal.</p> <p>End: SC centered under CM conveyor tail</p>
2	17.3	4.25	1.5	10.0	Target = 5 Person = 12	<p>CM: In straight Start: Centered, angled right</p> <p>End: SC under conveyor tail, but left of center, requiring CM conveyor tail to be swung to the left for achieving ideal loading position</p>

Test	Start Distance, m	End Distance, m	Min Step Size, m	Max Step Size, m	MinInit Dist, m	Comments
3	30	4.45	1	10.0	Target = 5 Person = 12	<p>Testing for correct reaction to person in the path and CM trammng forward.</p> <p>CM: In straight</p> <p>Start: Right rib</p> <p>Reaction to person: The path planner paused in all cases where the person was within the <i>minInitDistFrom Person</i> and resumed when the person moved beyond this distance.</p> <p>Reaction to CM trammng forward: After waypoint 3, SC was centered under conveyor tail. The CM was next trammed forward, causing it to exceed the <i>minInitDistFrom Target</i> and pipeline produced 2 additional waypoints to tram the SC forward.</p> <p>End: SC centered under conveyor tail</p>

Test	Start Distance, m	End Distance, m	Min Step Size, m	Max Step Size, m	MinInit Dist, m	Comments
4	20.9	4.4	1	10.0	Target = 5 Person = 12	CM: In right crosscut Start: Centered, angled slightly right End: SC centered under conveyor tail

## REFERENCES

- [1] Centers for Disease Control and Prevention. (n.d.). Number and percentage of occupational fatalities by accident class, 1998 - 2022 (N=1238). Centers for Disease Control and Prevention. <https://wwwn.cdc.gov/NIOSH-Mining/MMWC/Fatality/Count?StartYear=1998&EndYear=2022&SelectedMineType>.
- [2] “June 3, 2021 Fatality - Final Report.” *United States Department of Labor*, [www.msha.gov/data-reports/fatality-reports/2021/june-3-2021-fatality/final-report](http://www.msha.gov/data-reports/fatality-reports/2021/june-3-2021-fatality/final-report).
- [3] Burgess-Limerick, R., and L. Steiner. “Injuries associated with continuous miners, shuttle cars, load-haul-dump and personnel transport in New South Wales underground coal mines.” *Mining Technology*, vol. 115, no. 4, Dec. 2006, pp. 160–168, <https://doi.org/10.1179/174328606x151033>.
- [4] SENAPATI, Amrites, et al. “Associations of job-related hazards and personal factors with occupational injuries at continuous miner worksites in underground coal mines: A matched case-control study in indian coal mine workers.” *Industrial Health*, vol. 58, no. 4, 2020, pp. 306–317, <https://doi.org/10.2486/indhealth.2019-0102>.
- [5] Bauerle, Tim, et al. “Mineworker fatigue: A review of what we know and future decisions.” *Mining Engineering* vol. 70,3 (2018): 33.
- [6] LaValle, S. “Rapidly-Exploring Random Trees: A New Tool For Path Planning.” (1998). <https://msl.cs.uiuc.edu/~lavalle/papers/Lav98c.pdf>.
- [7] Arslan, Oktay, and Panagiotis Tsiotras. The Role of Vertex Consistency in Sampling-Based Algorithms for Optimal Motion Planning, 29 Apr. 2012. arXiv, <https://doi.org/10.48550/arXiv.1204.6453>.
- [8] Jaillet, L., et al. “Transition-based RRT for path planning in continuous cost spaces.” 2008 IEEE/RSJ International Conference on Intelligent Robots and Systems, 2008, <https://doi.org/10.1109/iros.2008.4650993>.
- [9] Nilsson, Nils J. *The Quest for Artificial Intelligence: A History of Ideas and Achievements*. Cambridge University Press, 2010.
- [10] Hart, Peter, et al. “A formal basis for the heuristic determination of minimum cost paths.” *IEEE Transactions on Systems Science and Cybernetics*, vol. 4, no. 2, 1968, pp. 100–107, <https://doi.org/10.1109/tssc.1968.300136>.
- [11] Scheduling, S., et al. “An experiment in autonomous navigation of an underground mining vehicle.” *IEEE Transactions on Robotics and Automation*, vol. 15, no. 1, 1999, pp. 85–95, <https://doi.org/10.1109/70.744605>.

- [12] Dragt, B J, et al. "An Overview of the Automation of Load-Haul-Dump Vehicles in an Underground Mining Environment." IFAC Proceedings Volumes, vol. 38, no. 1, 2005, pp. 37–48, <https://doi.org/10.3182/20050703-6-CZ-1902.01389>.
- [13] Losch, Robert, et al. "Design of an Autonomous Robot for Mapping, Navigation, and Manipulation in Underground Mines." 2018 IEEE/RSJ International Conference on Intelligent Robots and Systems (IROS), IEEE, 2018, pp. 1407–12, <https://doi.org/10.1109/IROS.2018.8594190>.
- [14] Remote Control Shuttle Car, <http://www.fent.us/technology-products/remote-control-shuttle-car/>.
- [15] Autonomous Shuttle Car, <http://www.fent.us/technology-products/autonomous-shuttle-car/>.
- [16] Agioutantis, Z., et al. "Lidar navigation in underground openings." Expanding Underground - Knowledge and Passion to Make a Positive Impact on the World, 12 Apr. 2023, pp. 2373–2380, <https://doi.org/10.1201/9781003348030-285>.
- [17] Miller, Sibley, "CONCEPTS FOR DEVELOPMENT OF SHUTTLE CAR AUTONOMOUS DOCKING WITH CONTINUOUS MINER USING 3-D DEPTH CAMERA" (2021). Theses and Dissertations--Mining Engineering. 68. [https://uknowledge.uky.edu/mng\\_etds/68](https://uknowledge.uky.edu/mng_etds/68).
- [18] Androulakis, Vasileios, "DEVELOPMENT OF AN AUTONOMOUS NAVIGATION SYSTEM FOR THE SHUTTLE CAR IN UNDERGROUND ROOM & PILLAR COAL MINES" (2021). Theses and Dissertations--Mining Engineering. 61. [https://uknowledge.uky.edu/mng\\_etds/61](https://uknowledge.uky.edu/mng_etds/61).
- [19] Rajvanshi, Abhinav, et al. "Autonomous docking using learning-based scene segmentation in Underground Mine Environments." 2022 IEEE International Symposium on Safety, Security, and Rescue Robotics (SSRR), 8 Nov. 2022, <https://doi.org/10.1109/ssrr56537.2022.10018611>.
- [20] Wada, K. Labelme: Image Polygonal Annotation with Python [Computer software]. <https://doi.org/10.5281/zenodo.5711226>.
- [21] "Equation of Circle When Three Points on the Circle Are Given." GeeksforGeeks, GeeksforGeeks, 13 Sept. 2023, [www.geeksforgeeks.org/equation-of-circle-when-three-points-on-the-circle-are-given/](http://www.geeksforgeeks.org/equation-of-circle-when-three-points-on-the-circle-are-given/).
- [22] "Pulse Width Modulation." Pulse Width Modulation - SparkFun Learn, [learn.sparkfun.com/tutorials/pulse-width-modulation/all](http://learn.sparkfun.com/tutorials/pulse-width-modulation/all).
- [23] "Servo - Writemicroseconds()." Servo - writeMicroseconds() - Arduino Reference, [www.arduino.cc/reference/en/libraries/servo/writemicroseconds/](http://www.arduino.cc/reference/en/libraries/servo/writemicroseconds/).

- [24] Kavraki, L.E., et al. “Probabilistic roadmaps for path planning in high-dimensional configuration spaces.” *IEEE Transactions on Robotics and Automation*, vol. 12, no. 4, 1996, pp. 566–580, <https://doi.org/10.1109/70.508439>.
- [25] Stentz, A. “Optimal and efficient path planning for partially-known environments.” *Proceedings of the 1994 IEEE International Conference on Robotics and Automation*, <https://doi.org/10.1109/robot.1994.351061>.
- [26] Janson, Lucas, et al. Fast Marching Tree: A Fast Marching Sampling-Based Method for Optimal Motion Planning in Many Dimensions. *arXiv*, <https://doi.org/10.48550/arXiv.1306.3532>.
- [27] Dijkstra, E. W. “A note on two problems in connexion with graphs.” *Numerische Mathematik*, vol. 1, no. 1, Dec. 1959, pp. 269–271, <https://doi.org/10.1007/bf01386390>.
- [28] Braun, João, et al. “A comparison of A\* and RRT\* algorithms with dynamic and real time constraint scenarios for Mobile Robots.” *Proceedings of the 9th International Conference on Simulation and Modeling Methodologies, Technologies and Applications*, 2019, <https://doi.org/10.5220/0008118803980405>.
- [29] Felmouba. *Occupancy Grid A Star*. (2018). GitHub Repository. <https://github.com/felmouba/occupancy-grid-a-star>.
- [30] “Scipy.Signal.Savgol\_filter” *Scipy.Signal.Savgol\_filter - SciPy v1.13.0 Manual*, [docs.scipy.org/doc/scipy/reference/generated/scipy.signal.savgol\\_filter.html](https://docs.scipy.org/doc/scipy/reference/generated/scipy.signal.savgol_filter.html).
- [31] Savitzky, Abraham., and M. J. Golay. “Smoothing and differentiation of data by simplified least squares procedures.” *Analytical Chemistry*, vol. 36, no. 8, 1 July 1964, pp. 1627–1639, <https://doi.org/10.1021/ac60214a047>.

VITA

Sky Rose

***Education:***

Computer Engineering  
Bachelor of Science

University of Kentucky  
Fall 2021

***Work Experience:***

Nyrstar Tennessee Mines  
Engineering Intern

May 2023 – August 2023

University of Kentucky  
Research Assistant

January 2022 – May 2024

Credit Solutions LLC  
IT Intern

June 2017 – December 2021

***Honors and Awards:***

Central Appalachian Regional Education Research Center Graduate Fellowship